A *MSTN*^{Del273C} mutation with *FGF5* knockout sheep by CRISPR/Cas9 promotes skeletal muscle myofiber hyperplasia via MEK-ERK-FOSL1 axis

Ming-Ming Chen[1, †], Yue Zhao[1, †], Xue-Ling Xu[1], Xiao-Sheng Zhang[2], Jin-Long Zhang[2], Su-Jun Wu[1], Zhi-Mei Liu[1], Yi-Ming Yuan[1], Xiao-Fei Guo[2], Shi-Yu Qi[1], Guang Yi[1], Shu-Qi Wang[1], Huang-Xiang Li[1], Ao-Wu Wu[1], Guo-Shi Liu[1], Kun Yu[1], Shoulong Deng[3], Hong-Bing Han[1], Feng-Hua Lv[1, *], Yan Li[4, *], Zheng-Xing Lian[1, *]

[1] Beijing Key Laboratory for Animal Genetic Improvement, National Engineering Laboratory for Animal Breeding, Key Laboratory of Animal Genetics and Breeding of the Ministry of Agriculture, College of Animal Science and Technology, China Agricultural University, Beijing 100193, China

[2] Institute of Animal Husbandry and Veterinary Medicine, Tianjin Academy of Agricultural Sciences, Tianjin 300381, China

[3] NHC Key Laboratory of Human Disease Comparative Medicine, Institute of Laboratory Animal Sciences, Chinese Academy of Medical Sciences and Comparative Medicine Center, Peking Union Medical College, Beijing, China

[4] Laboratory Animal Center of the Academy of Military Medical Sciences, Beijing 100071, China

† These authors contributed equally to this work.

* Correspondence: lianzhx@cau.edu.cn (Zheng-Xing Lian), scauly@cau.edu.cn (Yan Li); lvfenghua@cau.edu.cn (Feng-Hua Lv)

Abstract

Mutations in the well-known Myostatin (*MSTN*) produce a "double-muscle" phenotype, which makes it commercially invaluable for improving livestock meat production and providing high-quality protein for humans. However, mutations at different loci of the *MSTN* often produce a variety of different phenotypes. In the current study, we increased the delivery ratio of Cas9 mRNA to sgRNA from the traditional 1:2 to 1:10, which improves the efficiency of the homozygous mutation of biallelic gene. Here, a $MSTN^{Del273C}$ mutation with *FGF5* knockout sheep, in which the *MSTN* and *FGF5* dual-gene biallelic homozygous mutations were produced via the deletion of 3-base pairs of AGC in the third exon of *MSTN*, resulting in cysteine-depleted at amino acid position 273, and the *FGF5* double allele mutation led to inactivation of *FGF5* gene. The $MSTN^{Del273C}$ mutation with *FGF5* knockout sheep highlights a dominant "double-muscle" phenotype, which can be stably inherited. Both F0 and F1 generation mutants highlight the excellent trait of high-yield meat with a smaller cross-sectional area and higher number of muscle fibers per unit area. Mechanistically, the $MSTN^{Del273C}$ mutation with *FGF5* knockout mediated the activation of *FOSL1* via the MEK-ERK-FOSL1 axis. The activated *FOSL1* promotes skeletal muscle satellite cell proliferation and inhibits myogenic differentiation by inhibiting the transcription of MyoD1, and resulting in smaller myotubes.

Keywords: *MSTN*; *FGF5*; dual-gene biallelic mutation; *FOSL1*; myogenesis

1 Introduction

Myostatin (*MSTN*) has been well-known as a negative regulator of muscle growth and development. Its mutation produces a "double-muscle" phenotype, which shows its inestimable commercial value in improving meat production of livestock and poultry, and providing high-quality protein for humans (Fan *et al.*, 2022; Chen *et al.*, 2021b). Due to its role in promoting muscle atrophy and cachexia, *MSTN* has been recognized as a promising therapeutic target to offset the loss of muscle mass (Lee, 2021; Baig *et al.*, 2022; Wijaya *et al.*, 2022).

MSTN is highly conserved in mammals, and mutations in the *MSTN* gene, either artificially or naturally, will result in increased skeletal muscle weight and produce a "double-muscle" phenotype, which has been reported in many species, including cattle, sheep, and pigs, rabbits, and humans (Grisolia *et al.*, 2009; Dilger *et al.*, 2010; Kambadur *et al.*, 1997). However, mutations at different loci of the *MSTN* often produce variety of different phenotypes, and its molecular mechanism of skeletal muscle growth and development remains controversial (Hanset and Michaux, 1985; Grobet *et al.*, 1997; Wegner *et al.*, 2000; Kambadur *et al.*, 1997; Marchitelli *et al.*, 2003). More than 77 natural mutation sites of *MSTN* have been reported in various sheep breeds, most of these mutations were found to be located in the non-coding regions, and did not affect *MSTN* activity (Kijas *et al.*, 2007; Sjakste *et al.*, 2011; Han *et al.*, 2013; Dehnavi *et al.*, 2012). In addition to introns, it is still possible that mutations in regulatory regions and exons may not affect the sheep phenotypes (Pothuraju *et al.*, 2015; Kijas *et al.*, 2007; Boman and Vage, 2009; Boman *et al.*, 2009).

Fibroblast growth factor 5 (*FGF5*) belongs to the fibroblast growth factor (FGF) family and is a secretory signaling protein. *FGF5* played an inhibitory effect on mouse hair growth (Hebert *et al.*, 1994), and its natural mutation can lead to a significant increase in hair growth in angora mice (Sundberg *et al.*, 1997). Subsequent studies have also successively confirmed the inhibitory effect of *FGF5* on mammalian hair growth and is recognized to be a negative regulator of hair growth (Kehler *et al.*, 2007; Dierks *et al.*, 2013; Yoshizawa *et al.*, 2015; Legrand *et al.*, 2014; Higgins *et al.*, 2014).

FOS-like 1 (FOSL1), also named Fos-related antigen 1 (FRA1), is a member of the Fos subfamily of activator protein 1 (AP-1) superfamily. The Fos family proteins are involved in cell proliferation, differentiation, and transformation. FOSL1 and even AP-1 family members are generally recognized to be related to various cancers. However, accumulating evidence indicate that AP-1 family proteins play a critical role in skeletal muscle cell proliferation, differentiation, and muscle development (Puntschart *et al.*, 1998; Liu *et al.*, 2010). FOSL1 has also been characterized as an important component of the response of skeletal muscle during aging and a lipid biosynthesis-related factor (Mathes *et al.*, 2021; Wang *et al.*, 2017). Furthermore, FOSL2 and c-Jun, another member of the AP-1 family, were found to inhibit myoblast differentiation (Alli *et al.*, 2013; Bengal *et al.*, 1992). In all, it is foreseeable that the role of FOSL1 in myogenesis will increasingly emerge.

In this study, to increase both meat and wool production, we first produced the *MSTN* and *FGF5* dual-gene biallelic homozygous mutations sheep by the increased delivery ratio of Cas9 mRNA to sgRNA targeting *MSTN* and *FGF5*. The $MSTN^{Del273C}$ mutation with *FGF5* knockout sheep highlights a dominant "double-muscle" phenotype by decreasing the muscle fiber cross-sectional area and increasing the number of muscle fibers per unit area. Then, we used the *MSTN* and *FGF5* dual-gene biallelic homozygous mutations sheep to unravel the molecular mechanism of the "double-muscle" phenotype and myofiber hyperplasia.

2 Materials and Methods

2.1 Tissue sample collection and preparation

Gluteus medius and longissimus dorsi were harvested from WT and $MSTN^{Del273C}$ mutation with *FGF5* knockout ($MF^{-/-}$) sheep, and three WT sheep and four $MF^{-/-}$ F1 generation sheep (half-sib) were used for feeding and slaughter. All samples were immediately frozen in liquid nitrogen and then stored at −80°C until analysis. All sheep are raised by the national feeding standard NT/T815-2004. All procedures performed for this study were consistent with the National Research Council Guide for the Care and Use of Laboratory Animals. All experimental animal protocols in this study were approved and performed following the requirements of the Animal Care

110 and Use Committee at China Agricultural University (AW02012202-1-3). All
111 surgeries were performed under sodium pentobarbital anesthesia, and all efforts were
112 made to minimize any suffering experienced by the animals used in this study.

113 **2.2 Cell isolation, culture, and transfection**

114 Sheep skeletal muscle satellite cells were isolated and cultured as previously
115 described (Chen *et al.*, 2021a). In brief, the muscle tissues of the hind limbs from
116 3-month-old sheep fetuses were cut into small pieces, digested with 0.2% collagenase
117 type II (Gibco, Grand Island, NY) at 37℃ for 1 h, and then centrifuged at 1000 rpm
118 for 10 min. The precipitates were continued digested with 0.25% trypsin (Gbico,
119 Grand Island, NY) at 37℃ for 30 min, and digestion was terminated with serum
120 containing medium. The cell suspension was successively filtered through 100, 200
121 and 400 mesh cell sieves. After this, the cells were centrifuged at 1000 rpm for 10 min,
122 resuspended in growth medium (GM) containing DMEM/F12 (Gbico, Grand Island,
123 NY) with 20% fetal bovine serum (FBS, Gibco) and 1% penicillin-streptomycin
124 liquid (Gbico, Grand Island, NY), and cultured for 2-3 times with differential
125 adhesion. To induce differentiation, the cells were cultured to 70% confluence in GM,
126 and followed by an exchange to differentiation medium (DM) containing DMEM
127 high glucose (Gbico, Grand Island, NY) with 2% horse serum (HS, Gibco) and 1%
128 penicillin-streptomycin liquid to culture 24 h, 48 h, and 72 h. To produce viral
129 solution for over-expression of the target gene, it was subcloned into the XbaI and
130 BamHI sites of the lentiviral vector by seamless cloning. HEK 293T cells were
131 co-transfected with the envelope plasmid pMD2.G, the packaging plasmid psPAX2
132 and the target plasmid at a mass ratio of 1:2:4. Then, the culture medium was
133 collected at 48h and 72h after transfection, and the cell debris was removed by
134 filtration. Then, the sheep skeletal muscle satellite cells were infected with packaged
135 lentivirus when they were cultured to 60%-70% confluence in 96-well, 24-well or
136 6-well plates. Finally, cells were collected for analysis after infection at 24 h or 48 h.
137 All the primer sequences of gene cloning were listed in Table S1.

138 **2.3 Total RNA isolation and real-time quantitative PCR (RT- qPCR)**

139 The total RNA of tissues and cells was isolated using TRIzol reagent (Sangon
140 Biotech, Shanghai, China) following the manufacturer's protocol. In short, after
141 tissues or cells were lysed, chloroform was added to separate the organic and
142 inorganic phases, followed by precipitation with isopropanol and ethanol in turn, and
143 finally, the RNA was dissolved in DEPC water. Then, the first strand cDNA was
144 prepared using PrimeScript II 1st Strand cDNA Synthesis Kit (Takara, Beijing, China).
145 qPCR was performed using 2× SYBR Green qPCR Mix (Low ROX) (Aidlab
146 Biotechnologies, Beijing, Chian) in a Stratagene Mx3000P (Agilent Technologies,
147 SUA). With GAPDH mRNA as endogenous control, the relative expression level of
148 genes was calculated by the $2^{-\Delta\Delta Ct}$ method. All primers used were listed in Table S2.

149 **2.4 Western blot**

150 Tissue or cell samples were lysed in RIPA buffer (Solarbio, Beijing, China)
151 supplemented with protease and phosphatase inhibitor cocktail (Beyotime, Beijing,
152 China) for total protein extraction. Then, equal amounts of tissue or cell lysate were
153 resolved by 10% SDS-PAGE and transferred onto PVDF membranes (Millipore,
154 USA). The membranes were blocked with 5% BSA for 1h, incubated with primary
155 antibody at 4℃ overnight, then incubated with secondary antibody for 1h before
156 detection. The fold change of protein was normalized to GAPDH for quantitative
157 analysis by ImageJ software. The antibodies information was listed in Table S3.

158 **2.5 5-Ethynyl-2′-deoxyuridine (EdU) assay**

159 At 24 h after transfection, sheep skeletal muscle satellite cells were incubated at
160 37℃ for 2 h in 96-well plates with 50 μM EdU (RiboBio, Guangzhou, China). Then,
161 fixed the cells in 4% paraformaldehyde for 30 min and neutralized using 2 mg/mL
162 glycine solution. The Apollo® staining solution which contains EdU was added and
163 incubated at room temperature for 30 min in the dark to label the DNA in the
164 synthesis stage, the nuclear was then counterstained with DAPI. The number of EdU
165 positive cells was counted from the images of five random fields obtained with an

166 inverted fluorescence microscope at a magnification of 100×. EdU labeling index was
167 expressed as the number of EdU-positive cell nuclei/total cell nuclei.

168 **2.6 Cell counting kit-8 (CCK-8) and cell cycle detection**

169 Skeletal muscle satellite cells were seeded in 96-well plates and cultured for
170 appropriate time according to different experimental treatments. Then, 10 μL CCK-8
171 solution was added to each well and incubated at 37°C in a 5% CO_2 incubator for 2 h,
172 and then the absorbance at 450 nm was measured with a microplate reader.

173 The cultured skeletal muscle satellite cells were digested with trypsin,
174 centrifuged at 1000 g for 5 min to collect the cell pellet, washed once with ice-cold
175 PBS, and then 1 mL of ice-cold 70% ethanol was added to fix the cells overnight at
176 4°C. The next day, the cells were washed with ice-cold PBS again, and the cells were
177 incubated with 0.5 mL PI staining solution at 37°C for 30 min and collected by flow
178 cytometry at low speed.

179 **2.7 Immunofluorescence staining**

180 Sheep skeletal muscle cells were fixed in 4% paraformaldehyde for 30 min,
181 permeabilized in 0.1% Triton X-100 for 20 min and blocked with 5% normal goat
182 serum for 30 min at room temperature, and then incubated with primary antibody at 4℃
183 overnight. Next, the fluorescent secondary antibody was added and incubated at 37℃
184 for 1 h in the dark, and the nuclear was then counterstained with DAPI. The
185 immunofluorescence images from five random fields were captured with an inverted
186 fluorescence microscope.

187 **2.8 Chromatin Immunoprecipitation (ChIP)**

188 The cells were fixed with 1% formaldehyde for 10 min at room temperature, then
189 neutralized with 1× glycine solution for 5 min, and washed twice with ice-cold PBS.
190 Then, the cells were collected with a cell scraper and resuspended in 0.5 mL cell lysis
191 buffer (10 mM HEPES, 0.5% NP-40, 1.5 mM MgCl2, 10 mM KCl, pH 7.9)
192 containing protease inhibitor cocktail (Beyotime, Beijing, China) and incubated on ice
193 for 15 min to release the cytoplasm. Next, cell pellets were collected by centrifugation

at 800 g for 5 min at 4°C and resuspended in 0.5 mL nuclear lysis buffer (50 mM Tris, 10 mM EDTA, 0.3% SDS, pH 8.0) containing protease inhibitor cocktail. After the DNA was fragmented by ultrasonication, the suspension was centrifuged at 4°C 12000g for 10 min, and the supernatant was collected. And 50 μL supernatant of each sample was diluted with 450 μL of ChIP dilution buffer (0.01% SDS, 1.1% Triton X-100, 1.2 mM EDTA, 16.7 mM Tris-HCl pH 8.0, 167 mM NaCl), then 5 μg primary antibody was added and incubated overnight at 4°C with rotation. The next day, 20 μL protein A/G magnetic beads were added to each sample and incubated at 4°C with rotation for 2h. Then, the magnetic beads were respectively washed once with low-salt wash buffer (0.1% SDS, 1% Triton X-100, 2 mM EDTA, 20 mM Tris-HCl pH 8.0, 150 mM NaCl), high-salt wash buffer (0.1% SDS, 1% Triton X-100, 2 mM EDTA, 500mM NaCl, 20 mM Tris-HCl pH 8.0), LiCl wash buffer (0.25 M LiCl, 1% NP-40, 1% sodium deoxycholate, 1 mM EDTA, 10 mM Tris-HCl pH 8.0), and TE buffer (10 mM Tris-HCl pH 8.0, 1 mM EDTA) at 4°C, and the supernatant was discarded. Next, 100 μL ChIP elution buffer (1% SDS, 100 mM $NaHCO_3$) containing proteinase K was added to each sample, then incubated at 62°C overnight, and the DNA was finally purified by a purification column.

2.9 RNA-seq

The rRNA was removed from each total RNA sample of the gluteus medius to construct a strand-specific transcriptome sequencing library, and the Illumina Novaseq 6000 sequencing platform was used to perform high-throughput sequencing with a paired-end read length of 150 bp. Raw data were transformed into clean reads by removing reads containing adapter, ploy-N and low-quality reads from raw data. At the same time, Q20, Q30, GC-content, and sequence duplication levels of the clean data were calculated. The genome index was constructed using Hisat2 software and the clean reads were mapped to the sheep reference genome (*Oar Rambouillet v1.0*), the featureCounts software was used for expression quantification, and DESeq2 software was used for differential expression analysis based on P-value < 0.05 and | log2 Fold Change | > 1.

2.10 Statistical analysis

All results are presented as the mean ± SEM. Statistical analyses of differences between groups were performed using a two-tailed *Student's t*-test or chi-square test and $P < 0.05$ was considered statistically significant. $^{*}P < 0.05$, $^{**}P < 0.01$ and $^{***}P<0.001$.

3 Results

3.1 Elevated molar ratio of Cas9/sgRNA can efficiently generate biallelic homozygous mutant sheep

The sgRNAs for targeting were designed in the third exon of the MSTN and FGF5 genes, respectively, to generate mutant MSTN gene for quality trait improvement and mutant FGF5 gene for yield trait improvement sheep by CRISPR/Cas9 gene editing technology (Figure 1A, B). Both MSTN and FGF5 PCR products could be cleaved by T7E1 and the fragment sizes were also as expected, and grayscale analysis showed that the editing efficiency was 14.6% and 11.4%, respectively (Figure 1C), which indicates that the designed sgRNAs can achieve more efficient gene targeting.

The microinjection was performed according to the injection molar ratio of Cas9 mRNA:sgRNAs (1:2, 1:10, and 1:15), respectively. The number of embryos injected, recipients of nuclear transfer, pregnancy, and alive lambs per group were listed in Table S4. The subsequent gene mutation detection showed that a total of 3 lambs were mutated in the MSTN and FGF5 genes at a Cas9 mRNA:sgRNAs injection molar ratio of 1:2, with a gene editing mutation rate of 14.3% (4/28). However, all 3 lambs were chimeric, that is, there were both mutant and wild-type after editing, and the biallelic mutation rate was 0% (Table S4，Figure 1D). When the injection molar ratio of Cas9 mRNA:sgRNAs was 1:10, two lambs were mutated in MSTN and FGF5 genes, and the mutation rate of gene editing was 18.2 % (4/22). And these two lambs were all double-gene biallelic homozygous mutant lambs, that is, the alleles on the homologous chromosomes were mutated after the target gene was edited (Table S4, Figure 1D). While the injection molar ratio of Cas9 mRNA: sgRNAs was continuously increased to 1:15, one lamb had a mutation, which was a biallelic mutation of *MSTN* gene, and the gene editing mutation rate was 7.14% (1/14) (Table

254 S4, Figure 1D). All the mutation forms of bases and amino acids in MSTN and FGF5
255 genes are shown in Figure 1E and Figure 1F, respectively. These results indicate that
256 increasing the delivery molar ratio of Cas9 mRNA to sgRNA from 1:2 to 1:10 can
257 greatly improve the efficiency of biallelic mutation in sheep.

258 **3.2 The *MSTN*^{Del273C} mutation with *FGF5* knockout sheep highlights a dominant**
259 **"double-muscle" phenotype and muscle fiber hyperplasia**

260 Among gene-edited sheep, a sheep with biallelic deletion of *MSTN* and biallelic
261 mutation of *FGF5* aroused our great interest. Specifically, gene editing caused a
262 deletion of 3-base pairs of AGC in the third exon of *MSTN* (Figure 1E, F), resulting in
263 the deletion of cysteine at amino acid position 273 (*MSTN*^{Del273C}) (Figure 1 E, F),
264 which is highlighted by the "double-muscle" phenotype (Figure 2A, 2B). At the same
265 time, a biallelic mutation in *FGF5* caused the knockout of *FGF5* gene and increased
266 the density and length of hairs (Zhang *et al.*, 2020). Given the prominent
267 "double-muscle" phenotype of MF$^{-/-}$ sheep, we examined its histological morphology
268 of the gluteus medius and longissimus dorsi, and found that the fiber cell number per
269 unit area of muscle tissue in MF$^{-/-}$ sheep was significant (P<0.01) higher than that in
270 WT sheep (Figure 2C, D). Further, we also found that the percentage of smaller
271 myofiber in the gluteus medius and longissimus dorsi was clear higher in MF$^{-/-}$ sheep
272 than that in WT sheep, whereas the percentage of larger muscle fiber area was lower
273 (Figure 2C, E, F). To determine whether this phenomenon was affected by FGF5 gene
274 mutation, we also separately examined the muscle fiber morphology in FGF5
275 knockout sheep alone and found that FGF5 knockout alone had no significant (P>0.05)
276 effect on muscle fiber size (Figure S1). All these results demonstrated that the
277 dual-gene biallelic mutation MF$^{-/-}$ sheep had well-developed hip muscles with smaller
278 muscle fibers, and this phenotype was dominated by *MSTN* gene.

279 **Table 1 The slaughter traits of muscles in WT and MF$^{+/-}$ sheep**

Slaughter Indexes	WT (n=3)	MF$^{+/-}$ (n=4)	*P*-value
Live weight (kg)	56.33±3.088	50.15±2.058	0.14201
Carcass weight(kg)	32.23±2.436	28.5±1.588	0.23588
Slaughter percentage (%)	57.12±1.237	56.75±1.259	0.84403
loin muscle area (cm^2)	17.17±1.58	13.95±1.757	0.24795
Meat weight (kg)	18.79±1.306	15.68±0.825	0.08707

The proportion of meat in carcass	0.58±0.005	0.55±0.018	0.18691
The proportion of brisket and neck meat	0.14±0.018	0.13±0.004	0.85322
The proportion of loin meat	0.11±0.005	0.09±0.011	0.33339
The proportion of rib meat	0.22±0.004	0.15±0.003	0.00003
The proportion of foreleg meat	0.18±0.009	0.21±0.012	0.20974
The proportion of hind leg meat	0.33±0.009	0.4±0.016	0.0252
Neat percentage (%)	0.58±0.005	0.55±0.018	0.18691

To further determine the heritability of the above phenotypes, we crossed $MF^{-/-}$ sheep with homozygous WT sheep to produce the offspring generation of $MF^{-/-}$ sheep, which were identified that the gene editing could be stably inherited to the offspring, and they were all mutant heterozygotes of *MSTN* and *FGF5* monoalleles ($MF^{+/-}$) (Figure S2). Subsequently, 3 WT sheep and 4 $MF^{+/-}$ sheep were slaughtered. Compared to WT sheep, the proportion of rib meat was significantly reduced in $MF^{+/-}$ sheep, and the proportion of hind leg meat was significantly increased, the ratio of hind leg meat increased by 21.2% (Table 1). Further, the muscle weight of different parts in WT and $MF^{+/-}$ sheep has no significant difference (Table S5). However, the proportion of gluteus medius in the carcass of $MF^{+/-}$ sheep was significantly ($P<0.01$) increased, with a 26.3% increase compared to WT sheep (Figure 2G). In addition, there were no significant ($P>0.05$) differences in pH, color, drip loss, cooking loss, shearing force, and amino acid content of the longissimus dorsi between WT and $MF^{+/-}$ sheep (Table S6-8). Compared with WT sheep, the cross-sectional area of gluteus medius muscle fibers in $MF^{+/-}$ sheep was also smaller (Figure 2H-I), and the number of muscle fiber cells per unit area was significantly increased ($P<0.001$) (Figure 2H, J); the percentage of smaller muscle fiber area in $MF^{+/-}$ sheep was significantly increased ($P<0.05$), while the percentage of larger muscle fiber area was significantly decreased ($P<0.05$) (Figure 2H, K), these results was consistent with that in $MF^{-/-}$ sheep. All these results demonstrated that the dual-gene biallelic editing of the *MSTN* and *FGF5* could be stably inherited by the offspring, and the later generation characterized excellent traits of high-yield meat.

3.3 The *MSTN*^{Del273C} mutation with *FGF5* knockout promotes skeletal muscle satellite cells proliferation and inhibits myogenic differentiation

Given that the *MSTN*^{Del273C} mutation with *FGF5* knockout produced the phenotype of “double-muscle” and reduced muscle fiber cross-sectional area, we

306 detected the in-situ expression of MSTN protein. The results showed that there was no
307 significant differential expression of MSTN protein in both gluteus medius and
308 longissimus dorsi of $MF^{-/-}$ sheep compared with WT sheep (Figure S3A). Also, there
309 was no significant difference in MSTN mRNA (Figure S3B) and protein expression
310 (FigureS3C-D) in gluteus medius of WT and $MF^{+/-}$ sheep. Further
311 immunofluorescence also revealed no significant difference in MSTN protein
312 expression in both myoblasts and myotubes (Figure S3E). These results suggested that
313 the *MSTN*^{Del273C} mutation with *FGF5* knockout does not affect the normal expression
314 of *MSTN*.

315 The proliferation and differentiation of skeletal muscle satellite cells is a key step
316 in muscle formation and development. The CCK-8 and EdU cell proliferation
317 experiments showed that the proliferative rate of $MF^{+/-}$ cells were highly significantly
318 ($P<0.01$) elevated (Figure 3A) with a significant ($P<0.05$) increase in the rate of
319 EdU-positive cells (Figure 3B, C) compared to WT cells. In addition, cell cycle
320 detection showed a significant ($P<0.01$) reduce in the proportion of G1 phase and a
321 significant increase ($P<0.05$) in the proportion of S phase in $MF^{+/-}$ cells (Figure 3D,
322 E). Meanwhile, the mRNA expression levels of the cell cycle marker genes CyclinB1,
323 CDK4, Cyclin A1, Cyclin E1, and CDK2 were significantly increased ($P<0.05$)
324 (Figure 3F). These results suggest that the *MSTN*^{Del273C} mutation with *FGF5* knockout
325 may promote cell proliferation by accelerating the cell cycle from G0/G1 phase to S
326 phase.

327 Although the mRNA levels of MyoD1 and MyoG were significantly increased
328 after induced differentiation 2 days in $MF^{+/-}$ cells (Figure 3G), the mRNA level of
329 MyHC (Figure 3G) and the protein levels of MyoD1, MyoG, and MyHC (Figure 3H,
330 I) were dramatically decreased ($P<0.05$), suggesting that the $MSTN^{Del273C}$ mutation
331 with FGF5 inhibit myogenic differentiation. Meanwhile, the immunofluorescence
332 staining of MyoG and MyHC in myotubes showed that myotube fusion index (Figure
333 3J, K), number of myotubes (Figure 3J, L), and number of nuclei per myotube (Figure
334 3J, M) were all highly significantly ($P<0.01$) reduced after inducing differentiation for
335 2 days of $MF^{+/-}$ cells compared to WT cells, as was the myotube diameter at the
336 maximum measured (Figure 3J, N). To continue follow-up tracing of the progression

337 of myogenic differentiation, we also performed MyoG and MyHC
338 immunofluorescence staining after inducing differentiation for 4 days (DM4) and 6
339 days (DM6), and the results showed that the differentiation capacity and fusion ability
340 of $MF^{+/-}$ cells were consistently significantly lower than WT cells during the ongoing
341 differentiation process, as was the diameter of fused myotubes (Figure S4A-J). The
342 reduced expression of myogenic differentiation markers further confirmed that the
343 *MSTN*^{Del273C} mutation with *FGF5* knockout consistently inhibits myogenic
344 differentiation of skeletal muscle satellite cells (Figure S4K-N). Taken together, our
345 results elucidated that the *MSTN*^{Del273C} mutation with *FGF5* knockout inhibits
346 myogenic differentiation of skeletal muscle satellite cells and induces a smaller
347 myotube diameter of myotubes after induced differentiation, which may explain why
348 the cross-sectional area of muscle fibers is decreased in $MF^{-/-}$ and $MF^{+/-}$ sheep.

349 **3.4 FOSL1 is a key gatekeeper of *MSTN*^{Del273C} mutation with *FGF5***
350 **knockout-mediated muscle phenotype**

351 To elucidate the potential mechanism of the *MSTN*^{Del273C} mutation with *FGF5*
352 knockout result in smaller muscle fiber cross-sectional area and myotube diameter,
353 the RNA-seq was performed in gluteus medius. A total of 25,958 genes were
354 identified by RNA-seq, and principal component analysis (PCA) showed relatively
355 well repeatability within sample groups and well discrimination between WT and
356 $MF^{+/-}$ samples (Figure 4A). With P-value < 0.05 and | log2 Fold Change | > 1 as the
357 screening criterion, 295 differentially expressed genes (DEGs) were screened,
358 including 79 up-regulated DEGs and 216 down-regulated DEGs (Figure 4B). The
359 cluster analysis showed that the samples were clustered into WT groups and $MF^{+/-}$
360 groups, with obvious differences between groups (Figure 4C). Pearson correlation
361 analysis also showed high similarity within sample groups (Figure 4D).

362 GO enrichment analysis showed that 295 DEGs were significantly enriched in
363 signal transduction, positive regulation of cell proliferation, positive regulation of cell
364 migration, skeletal muscle cell differentiation, muscle contraction, cardiac muscle
365 contraction, and positive regulation of JNK cascade and so on in biological process
366 (BP); in cellular component (CC), these DEGs mainly belonged to cell membrane,
367 cytoplasm, perinuclear region of cytoplasm, and I band; and molecular function (MF)

368 mainly included protein binding, nucleotide binding, ATP binding, and protein kinase
369 activity (Figure 4E), indicating that these DEGs are significantly closely related to
370 cell proliferation, myogenic differentiation, and muscle development. In addition,
371 KEGG enrichment analysis showed that 295 DEGs were significantly enriched in
372 cytokine-cytokine receptor interaction, MAPK signaling pathway, IL-17 signaling
373 pathway, and TNF signaling pathway (Figure 4F), implying that DEGs were
374 significantly associated with cell proliferation, differentiation, apoptosis, and
375 inflammation. Furthermore, based on GO and KEGG enrichment analysis, 18 genes
376 with a large difference were selected from 295 DEGs for validation at mRNA level in
377 gluteus medius. The results showed that *GLIS1* was significantly ($P<0.05$)
378 up-regulated, and *MYL10*, *FOSL1*, *PDPN*, *PLA1A*, and *ANKRD2* were significantly
379 ($P<0.05$) down-regulated (Figure 4G).

380 In addition, we also verified the above six DEGs in the longissimus dorsi, in
381 which *FOSL1*, *PDPN* and *ANKRD2* were significantly ($P<0.05$) reduced in $MF^{+/-}$
382 sheep (Figure S5A). Given that $MSTN^{Del273C}$ mutation with *FGF5* knockout promotes
383 skeletal muscle satellite cell proliferation and inhibits differentiation, we dynamically
384 monitored the expression of *FOSL1*, *PDPN*, and *ANKRD2* during myogenic
385 differentiation. The results indicated that both *PDPN* and *ANKRD2* were significantly
386 ($P<0.05$) up-regulated during myogenic differentiation (Figure S5B-C). More
387 strikingly, *FOSL1* mRNA level was strongly ($P<0.01$) decreased after induced
388 differentiation (Figure 5A), and its expression diminished continuously with the
389 differentiation progress. Furthermore, compared with WT cells, the mRNA expression
390 levels of *FOSL1* in $MF^{+/-}$ cells at GM and DM2 were significantly ($P<0.05$) elevated
391 (Figure 5B), suggesting that *FOSL1* may play a crucial role in the proliferation and
392 myogenic differentiation of skeletal muscle satellite cells.

393 As aforementioned above, the AP-1 transcription factor family member c-Fos
394 inhibits myogenesis and MyoD1 expression by directly binding to the MyoD1
395 promoter region. Given that *FOSL1* is a member of the AP-1 family, we, therefore,
396 speculated that *FOSL1* might have similar functions to c-Fos. Subsequent
397 protein-protein interaction (PPI) analysis of FOSL1, c-Fos and MyoD1 further
398 suggested that there was a potential interaction between *FOSL1* and MyoD1 (Figure

399 5C). In addition, we also found that the mRNA expression level of c-Fos was highly
400 significantly (P<0.01) reduced in $MF^{+/-}$ myoblasts compared with WT cells, whereas
401 the expression level of MyoD1 mRNA was dramatically (P<0.01) increased (Figure
402 5D). Given the physical interaction between c-Fos and MyoD1, the JASPAR database
403 (https://jaspar.genereg.net/) was used to predict the binding of *FOSL1* to MyoD1
404 promoter region, and found that two bZIP recognition sites in the MyoD1 promoter
405 region had the most significant binding potential to FOSL1, of which motif 1 located
406 in the -1839 to -1830 region and motif 2 was located in the -1273 to -1264 region
407 (Figure 5E-G). Subsequently, ChIP-qPCR confirmed that FOSL1 directly binds to
408 these two bZIP recognition sites in the MyoD1 promoter region (Figure 5H-I),
409 indicating that FOSL1 plays an important role in the transcriptional regulation of
410 MyoD1.

411 **3.5 The *MSTN*^{Del273C} mutation with *FGF5* knockout contribute to muscle**
412 **phenotype via MEK-ERK-FOSL1 axis**

413 As previously mentioned, *FOSL1* may be a key gatekeeper of *MSTN*^{Del273C}
414 mutation with *FGF5* knockout-mediated muscle phenotype. Given that, we also
415 investigated the protein levels of *FOSL1* and c-Fos in GM and MD2, respectively. The
416 results showed that the protein level of *FOSL1* was significantly (P<0.05) reduced
417 and c-Fos protein levels were significantly (P<0.05) decreased in $MF^{+/-}$ cells at GM
418 compared with WT cells (Figure 6A-B), whereas FOSL1 protein levels were
419 significantly (P<0.05) diminished and c-Fos protein levels were highly significantly
420 (P<0.01) elevated in $MF^{+/-}$ cells after induced differentiation (Figure 6F-G), which
421 further demonstrated the key role of *FOSL1* on myogenesis. As demonstrated
422 previously, enrichment analysis significantly enriched the MAPK signaling pathway.
423 Compared with WT cells, the p-FOSL1 protein level of $MF^{+/-}$ cells was strongly
424 increased at GM (P<0.01) (Figure 6A-B), and there was no significant (P>0.05)
425 difference between MEK1/2 and p-MEK1/2 protein levels (Figure 6A, C), but its
426 downstream ERK1/2 protein level was extremely significantly (P<0.01) decreased,
427 and accompanied by a significant (P<0.05) increase in p-ERK1/2 protein levels
428 (Figure 6A, D). In addition, there was no significant (P>0.05) difference in p38
429 MAPK protein level, but p-p38 MAPK protein level was significantly (P<0.05)

430 enhanced (Figure 6A, E). After induced differentiation, there was no significant
431 (P>0.05) difference in p-FOSL1 protein level in $MF^{+/-}$ cells compared with WT cells
432 (Figure 6F-G), although both MEK1/2 and ERK1/2 protein levels were dramatically
433 (P<0.01) inhibited, there was no significant (P>0.05) difference in their
434 phosphorylated protein levels (Figure 6F, H-I). In addition, with a strong (P<0.01)
435 decrease in the p38 MAPK protein level, the p-p38 MAPK protein level dramatically
436 (P<0.01) increased (Figure 6F, J). These results suggested that *MSTN*^{Del273C} mutation
437 with *FGF5* knockout may regulate the expression and activity of *FOSL1* via the
438 MEK1/2-ERK1/2-FOSL1 axis to affect the proliferation and myogenic differentiation
439 of skeletal muscle satellite cells.

440 To investigate the role of *FOSL1* on the proliferation and myogenic
441 differentiation of skeletal muscle satellite cells, we successfully constructed *FOSL1*
442 gain-of-function model (Figure 7A, G-H). Our results showed that overexpression of
443 *FOSL1* significantly (P<0.01) increased the cell proliferation rate (Figure 7B), and the
444 mRNA expression levels of cell proliferation-related marker genes also significantly
445 (P<0.05) increased (Figure 7C). Meanwhile, the EdU cell proliferation assay further
446 demonstrated the promoting effect of *FOSL1* overexpression on cell proliferation
447 (Figure 7D-E). Similarly, we also investigated the expression of c-Fos and MyoD1,
448 respectively. As anticipated, the overexpression of *FOSL1* inhibited the MyoD1
449 mRNA (P<0.01) and protein (P<0.05) expression levels (Figure 7F, G-H), and
450 significantly (P<0.05) suppressed mRNA expression level of c-Fos (Figure 7F), and
451 we also observed a significant (P<0.01) increase in the expression level of p-FOSL1
452 protein (Figure 7G-H). These results are consistent with what we observed in $MF^{+/-}$
453 cells at GM, suggesting a potential inhibitory effect of p-FOSL1 protein levels on
454 MyoD1.

455 In addition, we also investigated the effect of *FOSL1*over-expression on cell
456 differentiation. Although the mRNA expression level of MyoG was significantly
457 increased (P<0.01) with an up-regulated tendency on MyoD1 mRNA, the expression
458 level of MyHC mRNA was significantly (P<0.05) reduced after FOSL1
459 overexpression (Figure 8A). More importantly, the protein expression levels of
460 MyoD1, MyoG and MyHC were all significantly decreased (P<0.05), proving that the

461 overexpression of FOSL1 inhibited the myogenic differentiation of skeletal muscle
462 satellite cells. Meanwhile, the p-FOSL1 protein expression level was also
463 significantly (P<0.01) elevated with the increase of FOSL1 protein expression level
464 (Figure 8B-C). Subsequently, immunofluorescence staining further confirmed the
465 significant (P<0.05) inhibitory effect of *FOSL1* overexpression on cell differentiation
466 (Figure 8D-E). Also, the number of myotubes, the number of nuclei per myotube, and
467 the myotube diameter all significantly decreased (P<0.05) (Figure 8D, F-H). These
468 results further demonstrated that elevated p-FOSL1 protein level inhibits myogenic
469 differentiation and produces smaller myotubes.

470 To further ascertain this insight, the tert-butylhydroquinone (TBHQ), which can
471 strongly activate ERK1/2 and increase p-ERK1/2 protein expression level, was used
472 to activate ERK1/2 and act as an indirect activator of FOSL1. As expected, the
473 addition of 20 μM TBHQ significantly (P<0.01) inhibited the myogenic
474 differentiation of skeletal muscle satellite cells (Figure 8I-J). And, the number of
475 myotubes was significantly increased (P<0.05) (Figure 8I, K), while the number of
476 nuclei per myotube was significantly (P<0.05) decreased and produced a smaller
477 myotube diameter (P<0.05) (Figure 8I, L-M). Taken together, these results repeatedly
478 confirm that FOSL1 as a key gatekeeper of $MSTN^{Del273C}$ mutation with FGF5
479 knockout-mediated muscle phenotype.

480 In short, our results shed light that the $MSTN^{Del273C}$ mutation with FGF5
481 knockout mediated the activation of FOSL1 via MEK-ERK-FOSL1 axis, further
482 promotes skeletal muscle satellite cell proliferation, and inhibits myogenic
483 differentiation by inhibiting the transcription of MyoD1, and resulting in smaller
484 myotubes (Figure 9). Our results demonstrate the potential mechanism for smaller
485 muscle fibers of $MSTN^{Del273C}$ mutation with *FGF5* knockout sheep.

486 4 Discussion

487 4.1 Optimized Cas9 mRNA and sgRNA delivery ratio improves the efficiency of 488 dual-gene biallelic homozygous mutations

489 The strategy for producing gene knockout animals by CRISPR/Cas9 gene editing
490 system is usually to introduce the Cas9 mRNA and the sgRNA of the target gene into

their prokaryotic embryos by microinjection. However, this “one-step” method often results in a “mosaic” of gene-edited offspring, that is, due to the fertilized egg will divide into multiple blastomeres successively many times, the editing ability and editing mode of the CRISPR/Cas9 system for each blastomere may be different, thereby resulting in the occurrence of chimeric mutant individuals carrying both the wild-type and mutant alleles (Wan *et al.*, 2015). Such chimeric mutants have now been reported in gene knockout mice (Wang *et al.*, 2013), rats (Bao *et al.*, 2015), monkeys (Niu *et al.*, 2014), pigs (Hai *et al.*, 2014), sheep (Hongbing HAN, 2014), goats (Wang *et al.*, 2015), rabbits (Lv *et al.*, 2016), and humans (Wang and Yang, 2019) prepared by a “one-step” method using the CRISPR/Cas9 system. For studies involved in genetic phenotypes, chimeric gene knockout animals require further cross-breeding to obtain animals with a complete knockout of the target gene. Once required to generate multiple gene knockout animals, this time-consuming and laborious operation will become extremely difficult. Although many studies have been devoted to eliminating this widespread chimeric mutation (Sato *et al.*, 2015; Sung *et al.*, 2014; Kotani *et al.*, 2015; Chen *et al.*, 2015; Zhou *et al.*, 2014; Tu *et al.*, 2017; Wang *et al.*, 2015), however, these optimizations did not bring about a significant improvement in the production efficiency of biallelic knockout animals. Here, we increased the delivery ratio of Cas9 mRNA to sgRNA from 1:2 to 1:10, which improve the efficiency of the homozygous mutation of the biallelic gene. This unprecedented optimization method not only improved the overall gene knockout efficiency, but also the obtained gene-edited offspring were all dual-gene biallelic mutation.

4.2 Phenotypes produced by *MSTN* mutations are mutation site-dependent

As mentioned previously, although *MSTN* mutations have been found to produce a “double-muscle” phenotype in multiple species, the microscopic phenotypes are different, and this difference is closely related to the mutation site and species types. In mice, the number of skeletal muscle fibers with *MSTN* gene knockout significantly increased by 86% (McPherron *et al.*, 1997). A missense mutant *MSTN* only increased the number of mouse muscle fibers, while dominant negative *MSTN* resulted in increased muscle fiber cross-sectional area in mice, but not the number of muscle

522 fibers (Nishi *et al.*, 2002; Zhu *et al.*, 2000). In addition, the use of *MSTN* neutralizing
523 antibody on adult rats also resulted in an increased muscle fiber cross-sectional area
524 (Haidet *et al.*, 2008). In cattle, natural MSTN mutant Belgian Blue cattle had an
525 increased number of muscle fibers and reduced muscle fiber diameter (Wegner *et al.*,
526 2000). The muscle fiber cross-sectional area of longissimus dorsi and gluteus medius
527 in sheep was significantly increased after a 4bp deletion of the first exon of *MSTN*
528 (Zhiliang *et al.*, 2004). In pigs, both the *MSTN* gene-edited Meishan and Hubei pigs
529 showed a phenotype with increased muscle fiber density (Qian *et al.*, 2015; Xu *et al.*,
530 2013). Here, we prepared $MSTN^{Del273C}$ mutation with *FGF5* knockout sheep with
531 3-base pairs of AGC in the third exon of *MSTN*, which caused the deletion of cysteine
532 at amino acid position 273. Its macroscopic phenotype is similar to that of the
533 MSTN-edited sheep with the first exon knocked out 4-base pairs. Both of them
534 showed an abnormally developed "double-muscle" phenotype of hip muscle, but the
535 microscopic phenotype was exactly the opposite.

536 **4.3 The phenotype of $MSTN^{Del273C}$ mutation with *FGF5* knockout sheep is only**
537 **controlled by *MSTN***

538 Although we produced the $MSTN^{Del273C}$ mutation with *FGF5* knockout sheep,
539 *FGF5* is currently recognized to be an important regulator of hair growth and
540 development and there is no direct evidence of a potential regulatory role of *FGF5* on
541 muscle development (Xu *et al.*, 2020; Zhang *et al.*, 2020; Higgins *et al.*, 2014; Hebert
542 *et al.*, 1994). Furthermore, there is no evidence of the crosstalk between *MSTN* and
543 *FGF5*. Importantly, we also did not find a significant effect on muscle fiber phenotype
544 in muscle morphological analysis of *FGF5* knockout alone sheep. These evidence
545 support whether it is homozygous mutant F0 generation or heterozygous mutant F1
546 generation, the reduction of muscle fiber cross-sectional area of $MSTN^{Del273C}$ mutation
547 with *FGF5* knockout sheep is only controlled by *MSTN*, whereas not *FGF5*. These
548 results indicate that *MSTN* may control skeletal muscle weight from two relatively
549 independent aspects regulating the number of muscle fibers during embryonic
550 development and the muscle fiber size after birth.

551 **4.4 The $MSTN^{Del273C}$ mutation with *FGF5* knockout activate *FOSL1* and promote**
552 **cell proliferation**

553 The proliferation and differentiation of skeletal muscle satellite cells is a key step
554 in myogenesis and muscle development, which is a highly coordinated multistep
555 biological process driven by many myogenic regulatory factors such as paired box
556 families (Pax3/7), myogenic regulatory factors (Myogenin, MyoD, Myf5, and
557 MRF4/6), myocyte enhancer factor 2 (MEF2) family proteins, these factors
558 collectively regulate the expression of muscle specific genes and to control skeletal
559 muscle development (Braun and Gautel, 2011). Aside from myogenic regulatory
560 factor, MSTN has been repeatedly demonstrated to be involved in the proliferation
561 (Thomas *et al.*, 2000b; Taylor *et al.*, 2001; Huang *et al.*, 2007; Ge *et al.*, 2020) and
562 differentiation (Langley *et al.*, 2002; Gao *et al.*, 2020) of skeletal muscle satellite cells.
563 MSTN negatively regulates the G1/S phase transition of cell cycle by specifically
564 up-regulating cyclin dependent kinase inhibitors p21WAF1/CIP1, and reducing the
565 level and activity of Cyclin-dependent kinase 2 (CDK2) protein in myoblasts
566 (Thomas *et al.*, 2000a; Joulia *et al.*, 2003; McCroskery *et al.*, 2003), resulting in the
567 arrest of myoblasts in G1 phase of cell cycle, so as to maintain the static state of
568 satellite cells. In this study, the $MSTN^{Del273C}$ mutation with *FGF5* knockout promoted
569 the transformation of G1/S phase by reducing the proportion of cell cycle G1 phase
570 and increasing the proportion of S phase, resulting in the activation of skeletal muscle
571 satellite cells and entry into the cell cycle, and further promoting cell proliferation.
572 Furthermore, *FOSL1* has been repeatedly proved to promote the proliferation of a
573 variety of cells, especially tumor cells (Sobolev *et al.*, 2022; Talotta *et al.*, 2020). In
574 the current study, the $MSTN^{Del273C}$ mutation with *FGF5* knockout led to the increase
575 of p-FOSL1 level, and the over-expression of *FOSL1* also promoted cell proliferation,
576 suggesting that the activated *FOSL1* is a key factor in the proliferation of skeletal
577 muscle satellite cells. Altogether, our results support that the $MSTN^{Del273C}$ mutation
578 with *FGF5* knockout promotes the proliferation of skeletal muscle satellite cells by
579 activating *FOSL1*.

580 **4.5 FOSL1 binds to the MyoD1 promoter and inhibits its transcription.**

581 In this study, AP-1 family member *FOSL1* was significantly reduced in $MF^{+/-}$
582 sheep, and its expression were drastically reduced during myogenic differentiation,
583 which was consistent with the decrease of *FOSL1* expression during C2C12

differentiation (Tobin *et al.*, 2016). Therefore, *FOSL1* was recognized as a potential gatekeeper. As mentioned previously, c-Fos, a member of the AP-1 transcription factor family, has been shown to inhibit myogenesis and MyoD1 expression by directly binding to the MyoD1 promoter region (Li *et al.*, 1992). Moreover, *FOSL1* heterodimerizes with other transcription factors, such as the members of the bZIP family, and these dimers are either disabling the transcriptional activator complex or saving the interacting proteins from degradation in proteasomes (Sobolev *et al.*, 2022). Therefore, we speculate that *FOSL1* may have similar functions to c-Fos. PPI analysis of *FOSL1*, c-Fos and MyoD1 suggested a potential interaction between *FOSL1* and MyoD1. Subsequently, we confirmed that FOSL1 directly binds to two bZIP recognition sites in the MyoD1 promoter region. Meanwhile, the overexpression of FOSL1 confirmed the potential inhibitory effect of FOSL1 and p-FOSL1 on MyoD1. In addition, FOSL2, another AP-1 family member, can also inhibit myoblast differentiation (Alli *et al.*, 2013), which may support the inhibitory effect of FOSL1 on myogenic differentiation. In a word, these results fully support our hypothesis that FOSL1 binds the MyoD1 promoter and inhibits its transcription.

4.6 The *MSTN*^{Del273C} mutation with *FGF5* knockout contribute to muscle phenotype via MEK-ERK-FOSL1 axis

MSTN dimer first binds to ActRIIB, and then binds to ALK4/5 to form a complex. Smad2/3/4 enters the nucleus to regulate the expression of target genes, and different transcription factors bind to Smad2/3/4 complex, resulting in different functions of Smad signaling pathway (Chen *et al.*, 2021b). The nonclassical pathway of MSTN involves PI3K/Akt/mTOR signaling pathway and MAPK signaling pathway, which mainly includes ERKs, JNKs and p38 MAPK (Huang *et al.*, 2007; Gui *et al.*, 2012). All of those pathways are involved in the signal transduction pathway of MSTN and mediate the transcription of MRFs (Myogenin, Myf5, MyoD), MuRF-1 and Atrogin-1, to regulate myogenic differentiation and skeletal muscle quality (Chen *et al.*, 2021b).

MSTN induces muscle fiber hypertrophy prior to satellite cell activation (Wang and McPherron, 2012) and inhibits IGF-I-induced increase in myotube diameter through Akt signaling pathway (Morissette *et al.*, 2009). Recently, a study on the

downstream target gene Smad2 of *MSTN* showed that the knock-out of Smad2 expression in primary myoblasts did not affect the efficiency of myogenic differentiation, but produced smaller myotubes with reduced expression of the terminal differentiation marker myogenin. In turn, the overexpression of Smad2 stimulated the expression of myogenin and enhanced cell differentiation and fusion (Lamarche *et al.*, 2021). In our study, the $MSTN^{Del273C}$ mutation with FGF5 knockout resulted in the inhibition of myogenic differentiation of skeletal muscle satellite cells, and the number of myotubes and the myotube size were significantly reduced.

As previously described, the DEGs of gluteus medius RNA-seq were significantly enriched in the MAPK signaling pathway. A recent study on glioma showed that FOSL1 can be activated by the Ras-MEK1/2-ERK1/2 axis in MAPK signaling pathway (Marques *et al.*, 2021). Similarly, the activated MEK1/2-ERK1/2 axis in aged skeletal muscle also activates FOSL1 and increases the abundance of FOSL1 and the trans-activation capacity of the Fos-Jun heterodimer (Mathes *et al.*, 2021). In our study, the $MSTN^{Del273C}$ mutation with FGF5 knockout regulates FOSL1 expression and activity through MEK1/2-ERK1/2-FOSL1 axis and activated FOSL1 further inhibits myogenic differentiation of skeletal muscle satellite cells, resulting in smaller myotube diameter. However, puzzlingly, despite the high expression of p-FOSL1 in $MF^{+/-}$ myoblasts, it did not significantly inhibit the transcription of MyoD1, which may be related to a dramatic enhance in c-Fos, or there might be other signaling pathways regulating MyoD1 after $MSTN^{Del273C}$ mutation with FGF5 knockout. Furthermore, it has been demonstrated that the inhibition of MEK1/2 using MEK1/2-specific inhibitor PD184352 can significantly down-regulate FOSL1 expression (Mathes *et al.*, 2021). To further confirm our hypothesis, TBHQ was used to activate ERK1/2 and act as an indirect activator of FOSL1. Interestingly, activated FOSL1 markedly inhibited myogenic differentiation of skeletal muscle satellite cells, which also resulted in smaller myotubes, but significantly increased the number of myotubes. Taken together, these results shed light on the potential mechanisms by which $MSTN^{Del273C}$ mutation with FGF5 knockout leads to increased myofiber numbers and decreased fiber cross-sectional area.

5 Conclusion

646 In this study, we found that increasing the delivery ratio of Cas9 mRNA to
647 sgRNA can improve the efficiency of the homozygous mutation of the biallelic gene.
648 Based on this, we generated a *MSTN*^{Del273C} mutation with *FGF5* knockout sheep, a
649 dual-gene biallelic homozygous mutant, which highlights a dominant "double-muscle"
650 phenotype. Both F0 and F1 generation mutants highlight the excellent trait of
651 high-yield meat and the more number of muscle fibers per unit area. Our results
652 suggested the MSTN^{Del273C} mutation with FGF5 knockout mediated the activation of
653 FOSL1 via MEK-ERK-FOSL1 axis, further promotes skeletal muscle satellite cell
654 proliferation, and inhibits myogenic differentiation by inhibiting the transcription of
655 MyoD1, and resulting in smaller myotubes. This supports the myofiber hyperplasia
656 that more number of muscle fibers and smaller cross sectional area, caused by the
657 MSTN^{Del273C} mutation with FGF5 knockout.

658 **Data availability statement**

659 The raw sequence data reported in this paper have been deposited in the Genome
660 Sequence Archive (Genomics, Proteomics & Bioinformatics 2021) in National
661 Genomics Data Center (Nucleic Acids Res 2022), China National Center for
662 Bioinformation / Beijing Institute of Genomics, Chinese Academy of Sciences (GSA:
663 CRA008539) that are publicly accessible at https://ngdc.cncb.ac.cn/gsa.

664 **Ethics statement**

665 All experiments were performed in accordance with relevant guidelines and
666 adhere to the ARRIVE guidelines (https://arriveguidelines.org/) for the reporting of
667 animal experiments. All sheep are raised in accordance with the national feeding
668 standard NT/T815-2004. All procedures performed were consistent with the National
669 Research Council Guide for the Care and Use of Laboratory Animals. All
670 experimental animal protocols were approved and performed in accordance with the
671 requirements of the Animal Care and Use Committee at China Agricultural University
672 (AW02012202-1-3).

673 **Competing financial interests**

674 The authors declare that there are no competing financial interests.

675 **Author contributions**

MMC performed the majority of experiments, data analysis, and drafted the manuscript. YZ performed a part of experiments and revised the manuscript. XLX, SJW and ZML helped with data analysis. XSZ, JLZ and XFG were responsible for the management of the feeding plant, slaughtering, and collecting samples. YMY helped to process some biological information data. SYQ, GY, SQW, HXL and AWW helped to collect and organize original data. GSL led the prokaryotic injection and embryo transfer. YL prepared the gene editing sheep. KY and HBH participated in project management. KY, FHL and ZXL conceived the project, revised manuscript and final approval of manuscript. All authors read and approved the final manuscript.

Acknowledgments

This work was supported by National Key Research and Development Program-Key Projects (2021YFF1000704, 2021YFD1200900), Natural Science Foundation of China (32072722), and National Transgenic Creature Breeding Grand Project (2016zx08008-003).

691 **Figure Legends**

692 **Figure 1 Efficient generation of sheep carrying biallelic mutations in dual gene**
693 **via the CRISPR/Cas9 system**

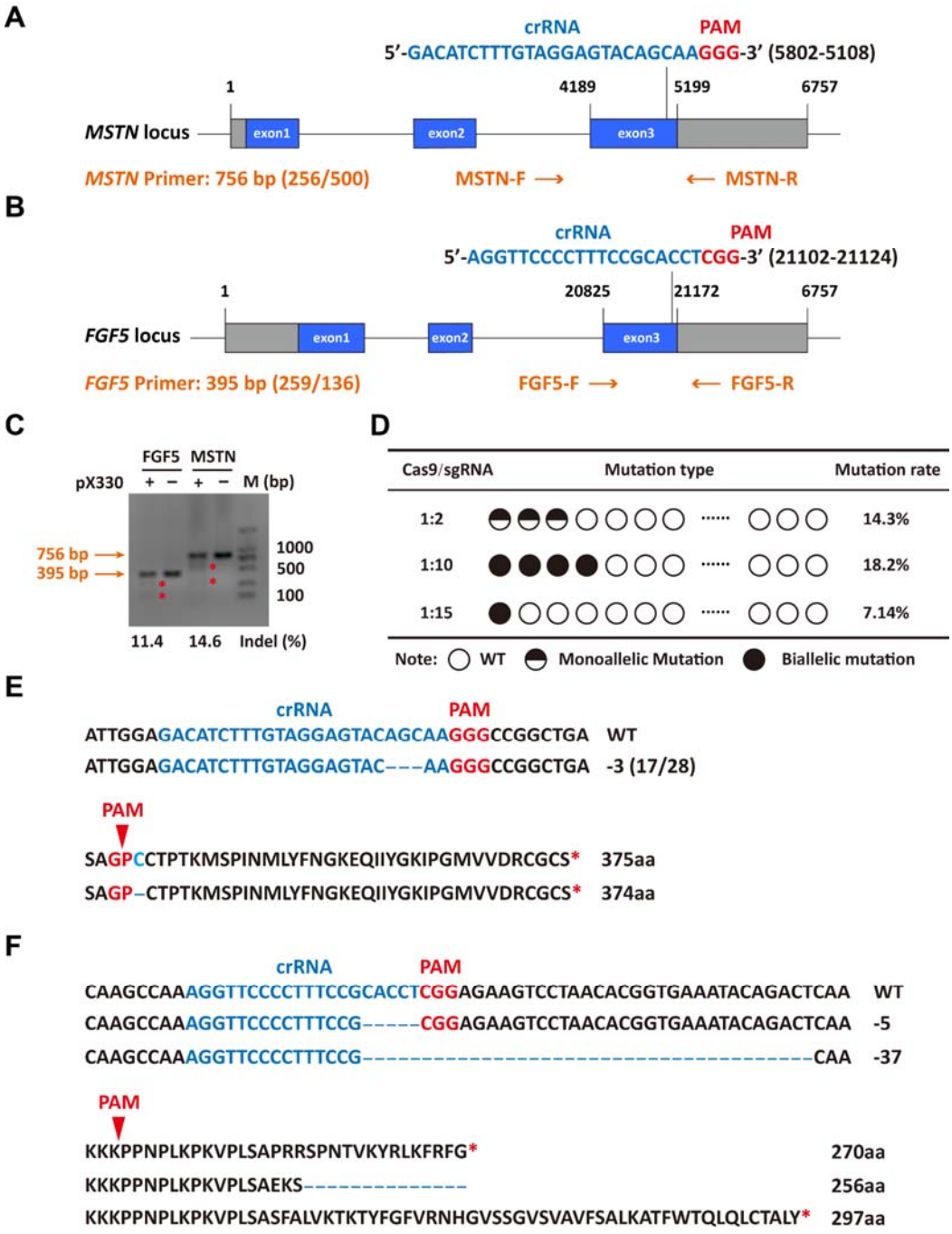

694

695 (A) Schematic of sgRNAs specific to exon 3 of the sheep MSTN locus. The crRNA
696 sequences are highlighted in blue typeface and the PAM in red. (B) Schematic of
697 sgRNAs specific to exon 3 of the sheep FGF5 locus. The crRNA sequences are

698 highlighted in blue typeface and the PAM in red. (C) T7EI assay for sgRNAs of
699 MSTN and FGF5 in sheep fetal fibroblasts. The cleavage bands are marked with an
700 red asterisk (*) and the indel frequencies were calculated using the expected
701 fragments. (D) Summary of the generation of sheep carrying biallelic mutations in
702 dual gene via zygote injection of Cas9 mRNA/sgRNAs. (E) Analysis of genome
703 sequence and amino acid sequence of MSTN-modified sheep. The location of sgRNA
704 and PAM are highlighted in blue and red, respectively. The deletions are indicated by
705 a dashed line (-). (F) Analysis of genome sequence and amino acid sequence of
706 FGF5-modified sheep. The location of sgRNA and PAM are highlighted in blue and
707 red, respectively. The deletions are indicated by a dashed line (-).
708
709

Figure 2 The *MSTN*^{Del273C} mutation with *FGF5* knockout sheep highlights a dominant "double-muscle" phenotype and muscle fiber hyperplasia

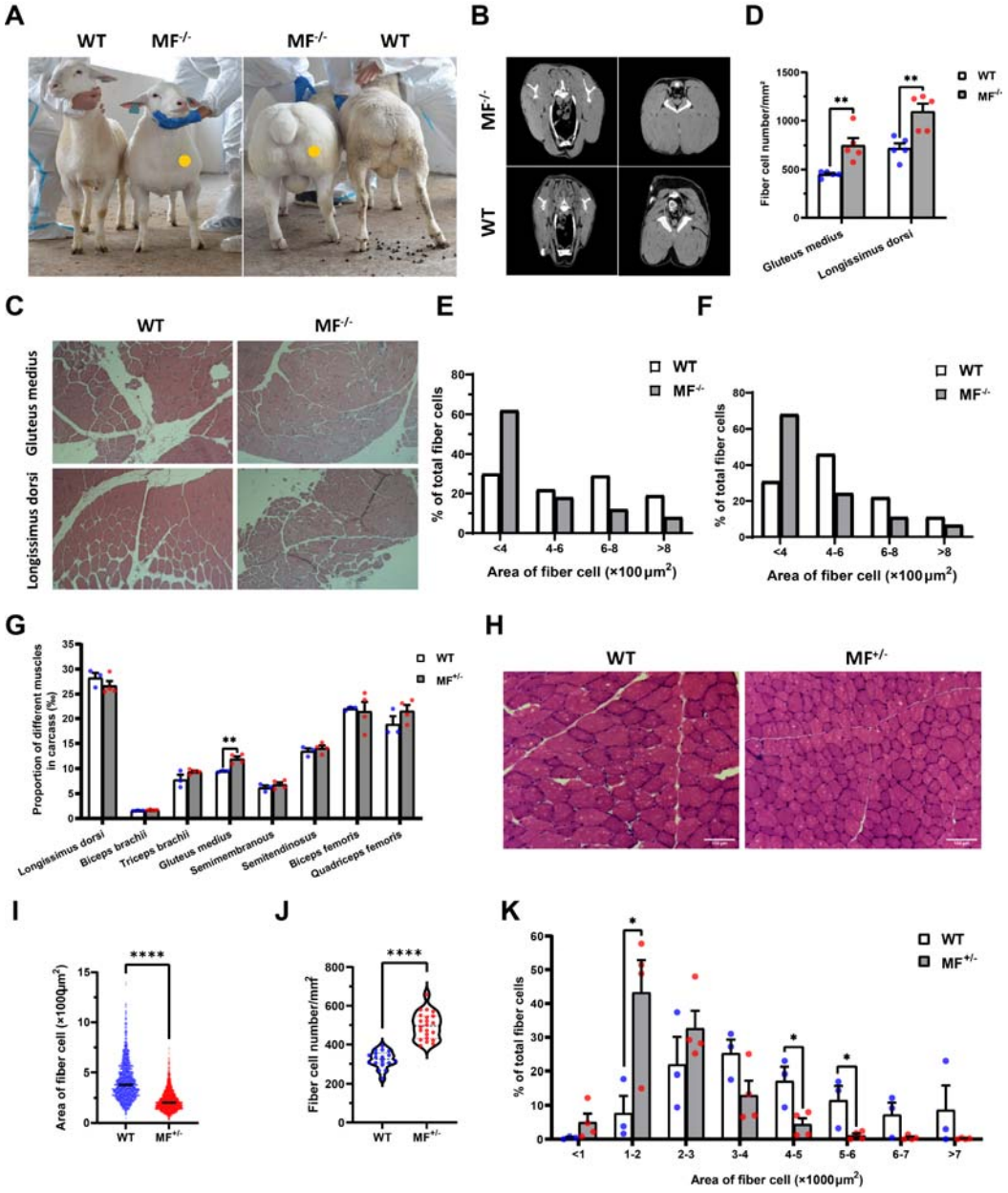

(A) The 6-month-old WT and MF$^{-/-}$ sheep. The genome-edited sheep displayed an obvious "double-muscle" phenotype compared with the WT. (B) The CT scanning image of the brisket and hip of WT and MF$^{-/-}$ sheep. (C) HE sections of gluteus medius and longissimus dorsi of WT and MF$^{-/-}$ sheep. Scale bar 100 μm. (D) Quantification of muscle fibre cell number of per unit area in WT and MF$^{-/-}$ sheep. (E-F) The percentage of cross-sectional area of different size muscle fibers in all

719 muscle fibers. (G) The proportion of different muscles in carcass in WT and $MF^{+/-}$
720 sheep. (H) HE sections of gluteus medius in WT and $MF^{+/-}$ sheep. Scale bar 100 μm.
721 (I) Quantification of muscle fibre cell area of gluteus medius in WT and $MF^{+/-}$ sheep.
722 (J) Quantification of muscle fibre cell number of per unit area in WT and $MF^{+/-}$ sheep.
723 (K) The percentage of cross-sectional area of different size muscle fibers.
724
725

Figure 3 The MSTN^{Del273C} mutation with FGF5 knockout promote proliferation and inhibit differentiation of skeletal muscle satellite cells

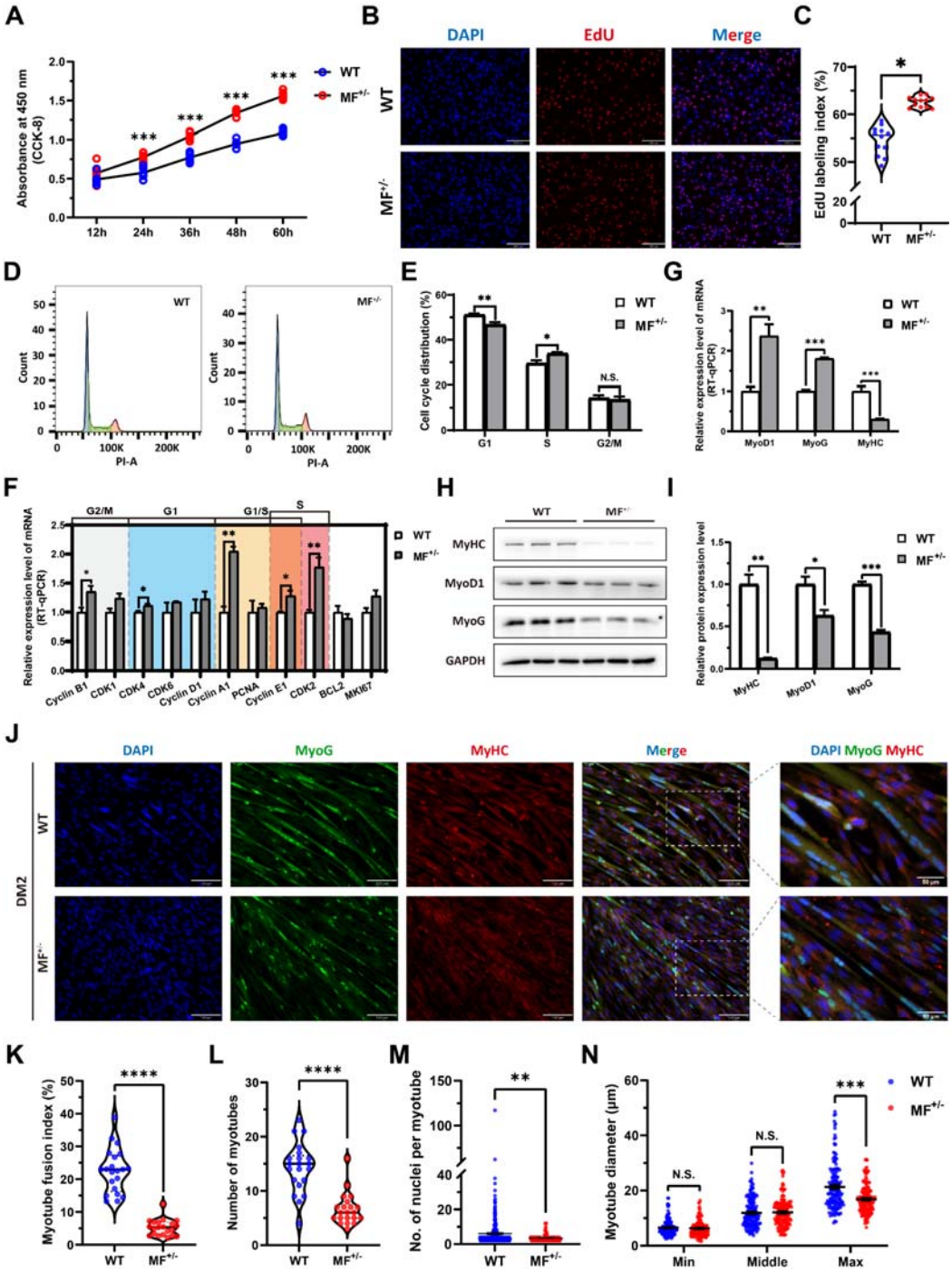

(A) The number of cells was detected by CCK-8 at 12h, 24h, 36h, 48h, and 60h in GM. (B-C) EdU assay showed that the number of EdU positive cells and EdU labeling index were significantly increased in MF$^{+/-}$ cells. Scale bar 130 μm. (D-E) PI

732 staining to detect cell cycle and showed a significant reduce in the proportion of G1
733 phase and a significant increase in the proportion of S phase in $MF^{+/-}$ cells. (F) The
734 mRNA expression levels of cell cycle marker genes and cell proliferation marker
735 genes. (G) The mRNA expression levels of myogenic differentiation marker genes
736 MyoG, MyoD1, and MyHC. (H-I) The protein expression levels of myogenic
737 differentiation marker genes MyoG, MyoD1, and MyHC. (J) The MyoG and MyHC
738 immunofluorescence staining of myotubes in DM2. Scale bar 130 μm. (K) The
739 myotube fusion index, which was represented by the number of cell nuclei in
740 myotubes/total cell nuclei. (L) The number of myotubes, which was the number of all
741 myotubes in the field of view. (M) The number of nuclei per myotube. (N) The
742 myotube diameter. To reflect the myotube diameter as accurately as possible, the
743 vertical line at the thinnest position of the myotube is taken as the minimum measured
744 (Min), the mid-perpendicular line of the long myotube axis is taken as the middle
745 measured (Middle), and the vertical line at the widest position of the myotube is taken
746 as the maximum measured (Max).
747
748

Figure 4 Identification of potential regulators by RNA-seq

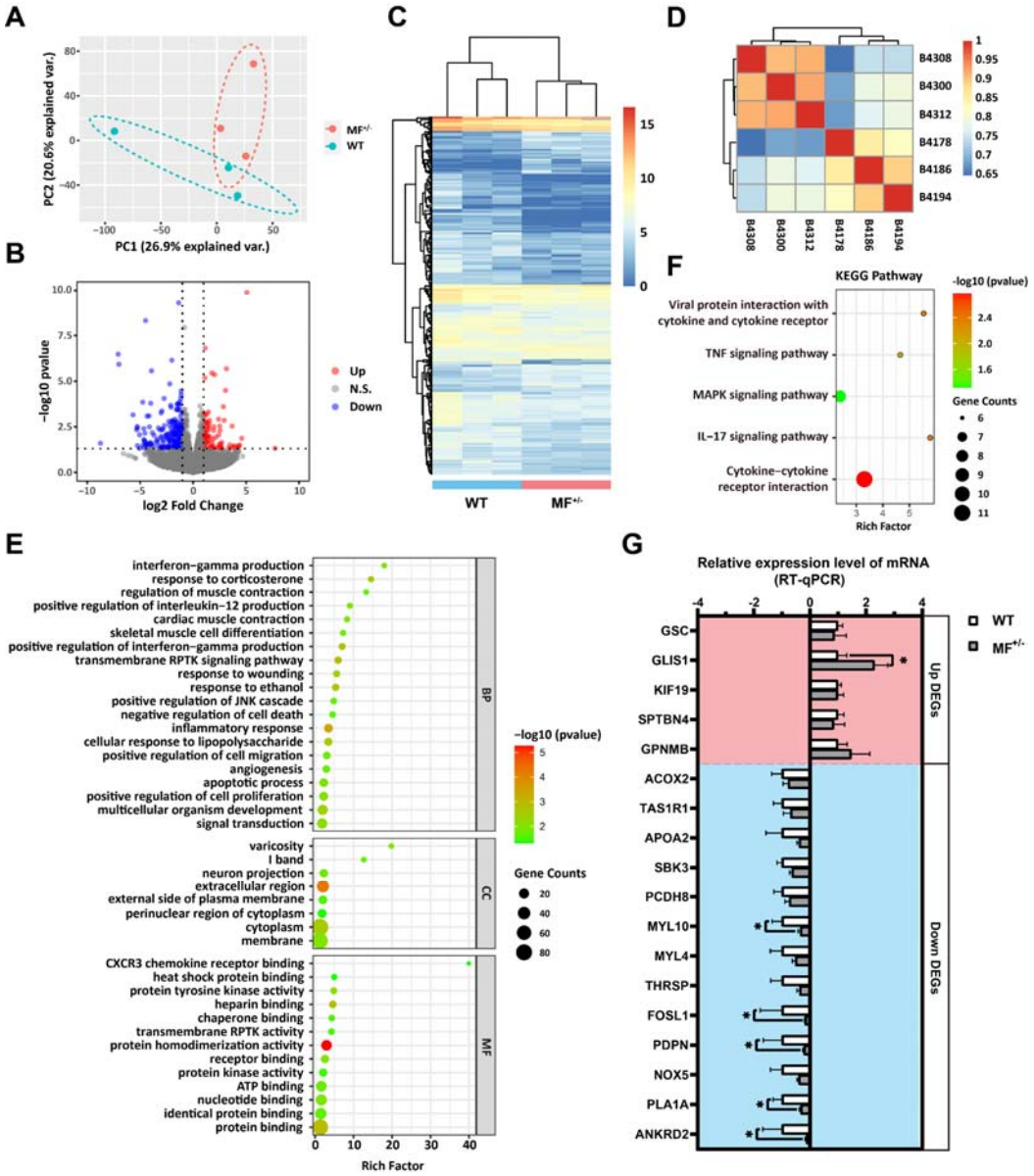

(A) Principal component analysis (PCA) of six gluteus medius samples in WT and $MF^{+/-}$ sheep. (B) Volcano plot of differentially expressed genes (DEGs) between WT and $MF^{+/-}$ sheep. The up- and down-regulated DEGs are shown in red and blue, respectively. (C) The heat map of DEGs between WT and $MF^{+/-}$ sheep. (D) Pearson correlation analysis between samples. (E) Go enrichment analysis of DEGs. Among them, the top 20 entries with significant enrichment are listed in biological process (BP). CC, cellular component; MF, molecular function. (F) KEGG enrichment analysis of DEGs. (G) The expression verification of DEGs by RT-qPCR.

759

760 **Figure 5 *FOSL1* may regulate myogenesis by binding to the MyoD1 promoter**
761 **region**

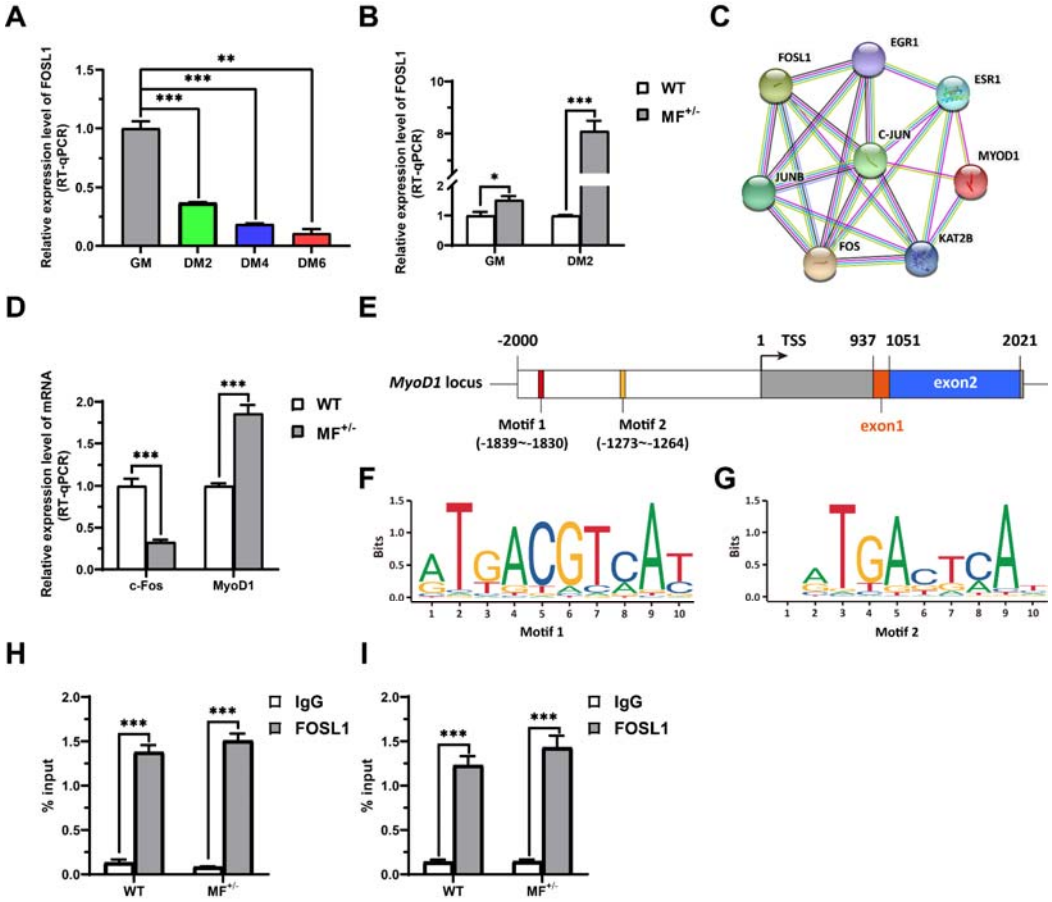

762

763 (A) The expression level of FOSL1 mRNA during myogenic differentiation. (B) The
764 mRNA expression levels of FOSL1 both at GM and DM2 in WT and $MF^{+/-}$ cells. (C)
765 The protein-protein interaction (PPI) analysis of FOSL1, c-Fos and MyoD1. (D) The
766 mRNA expression level of c-Fos and MyoD1 at GM in WT and $MF^{+/-}$ myoblasts. (E)
767 Schematic diagram of MyoD1 gene body, promoter region and binding sites. (F-G)
768 FOSL1 recognition motif in the MyoD1 promoter region. (H) FOSL1 ChIP-qPCR of
769 motif 1 recognition region. (I) FOSL1 ChIP-qPCR of motif 2 recognition region.

770

771

Figure 6 The *MSTN*^{Del273C} mutation with *FGF5* knockout contributes to muscle phenotype via MEK-ERK-FOSL1 axis

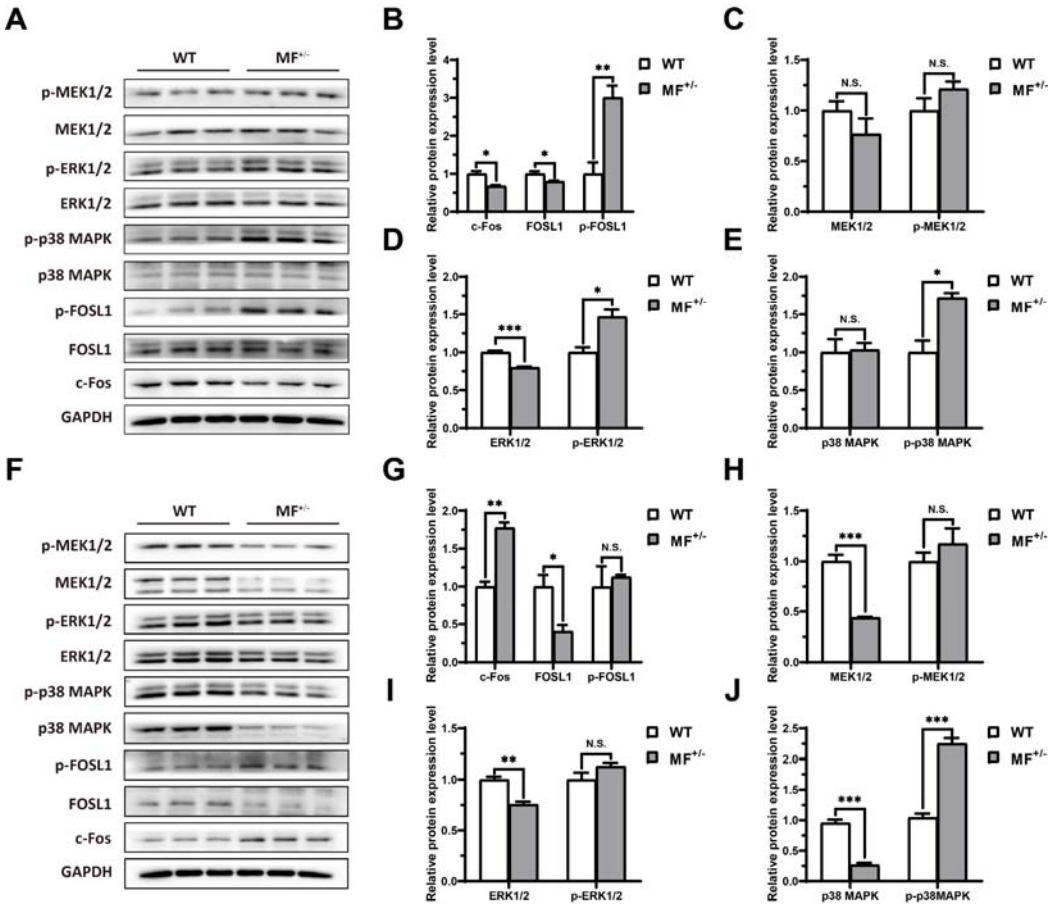

(A) Western blot of FOSL1, c-Fos, and key kinases of MAPK signaling pathways in GM. (B-E) Quantification of protein expression of FOSL1, c-Fos, and key kinases of MAPK signaling pathways in GM. (F) Western blot of FOSL1, c-Fos, and key kinases of MAPK signaling pathways in DM2. (G-J) Quantification of protein expression of FOSL1, c-Fos, and key kinases of MAPK signaling pathways in DM2.

782 **Figure 7 *FOSL1* overexpression promotes the proliferation of skeletal muscle**
783 **satellite cells**

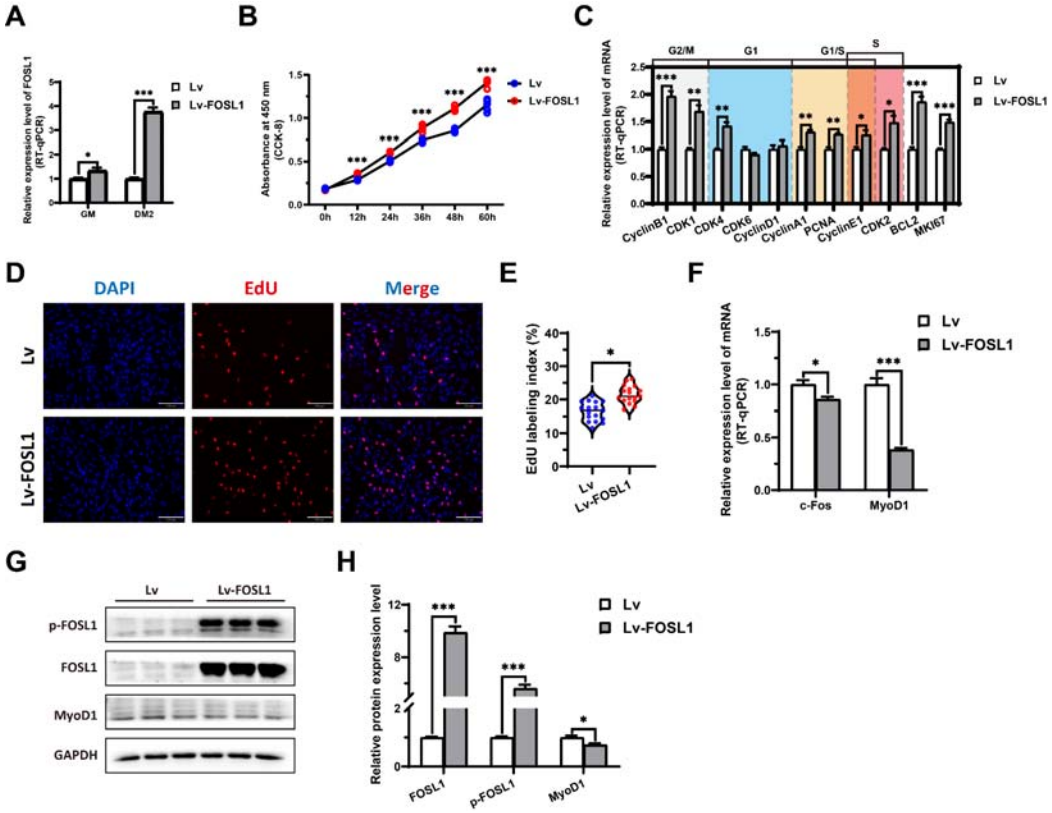

784

785 (A) The mRNA expression level of FOSL1 at GM and DM2 after lentivirus infection.
786 (B) The number of cells detected by CCK-8 at 0h, 12h, 24h, 36h, 48h, and 60h after
787 infection with lentivirus. (C) The mRNA expression levels of cell cycle marker genes
788 and cell proliferation marker genes. (D-E) EdU assay showed that the number of EdU
789 positive cells and EdU labeling index were significantly increased after infection with
790 lentivirus. Scale bar 130 μm. (F) The mRNA expression levels of c-Fos and MyoD1 at
791 GM after FOSL1 overexpression. (G-H) The protein expression levels of FOSL1,
792 p-FOSL1 and MyoD1 at GM after FOSL1 overexpression.

793

794

Figure 8 Highly expressed or activated FOSL1 inhibits myogenic differentiation

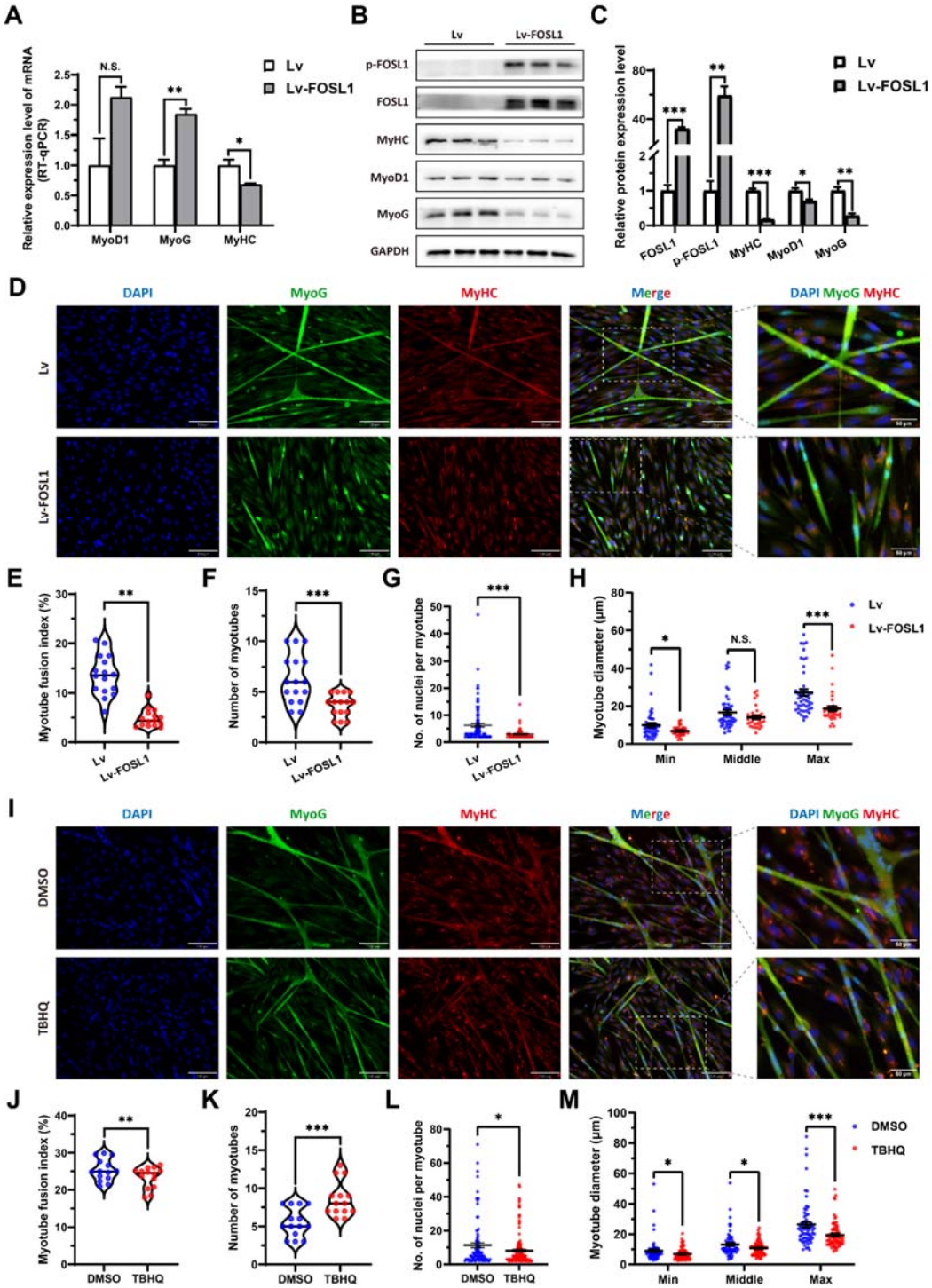

(A) The mRNA expression levels of myogenic differentiation marker genes MyoD1, MyoG and MyHC at DM2 after overexpression of FOSL1. (B-C) The protein expression levels of FOSL1, p-FOSL1 and myogenic differentiation marker genes

800 MyoD1, MyoG and MyHC at DM2 after overexpression of FOSL1. (D) The MyoG
801 and MyHC immunofluorescence staining of myotubes at DM2 after overexpression of
802 FOSL1. Scale bar 130 μm. (E-H) The myotube fusion index, number of myotubes,
803 number of nuclei per myotube and the myotube diameter at DM2 after overexpression
804 of FOSL1. (I) The MyoG and MyHC immunofluorescence staining of myotubes at
805 DM2 after addition of 20 μM TBHQ. Scale bar 130 μm. (J-M) The myotube fusion
806 index, number of myotubes, number of nuclei per myotube and the myotube diameter
807 at DM2 after the addition of 20 μM TBHQ.
808
809

810 **Figure 9 Schematic illustration of the regulation of muscle phenotypes by**
811 ***MSTN*^{Del273C} mutation with *FGF5* knockout**

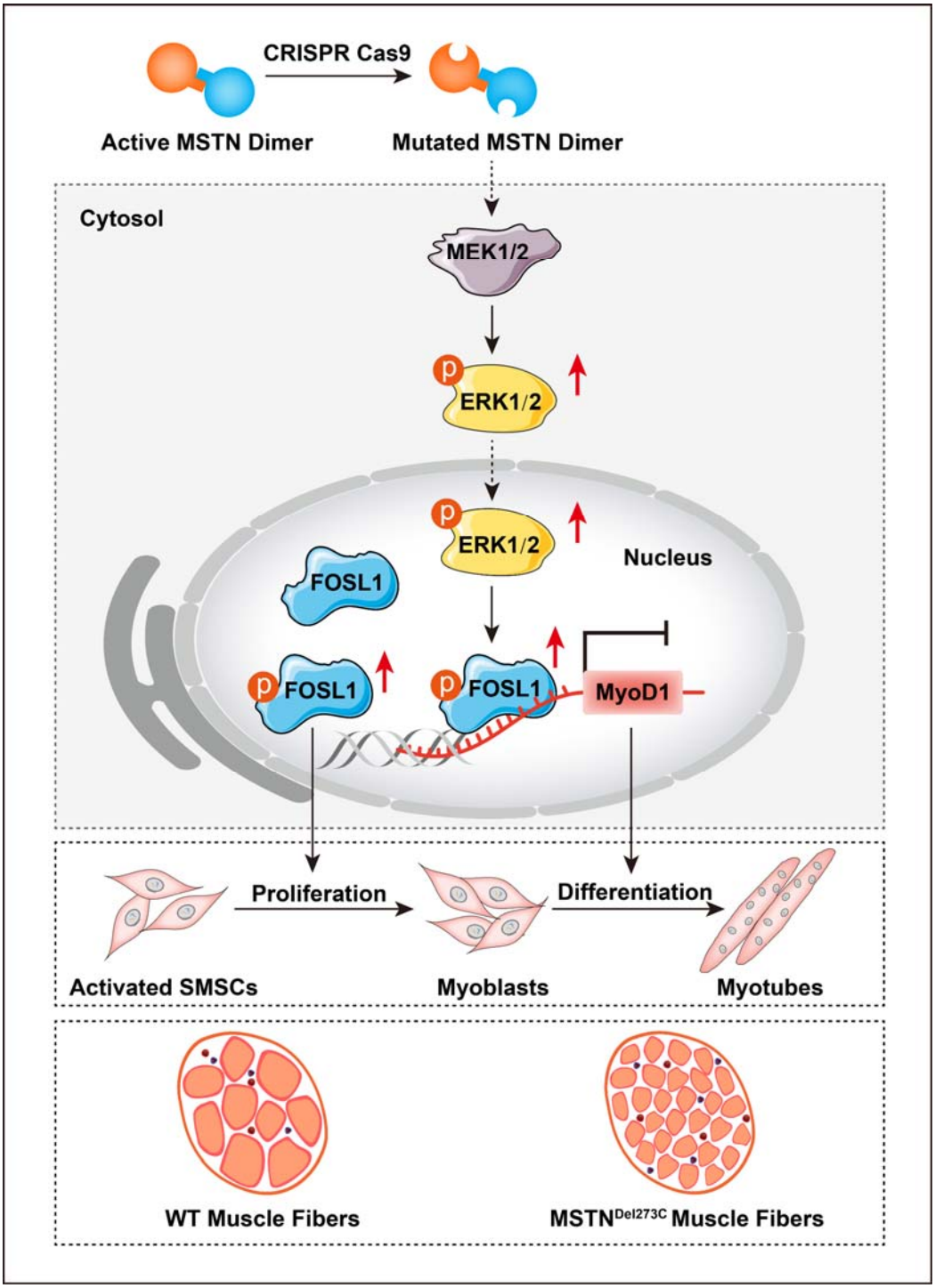

812

813 The *MSTN*^{Del273C} mutation with *FGF5* knockout mediated the activation of
814 FOSL1 via MEK-ERK-FOSL1 axis. The activated FOSL1 further promotes skeletal

815 muscle satellite cell proliferation and inhibits myogenic differentiation, and resulting
816 in smaller myotubes, which demonstrates the potential mechanism for smaller muscle
817 fibers of *MSTN*^{Del273C} mutation with *FGF5* knockout sheep.
818
819 **Figure S1 *FGF5* mutation does not affect muscle fiber size**

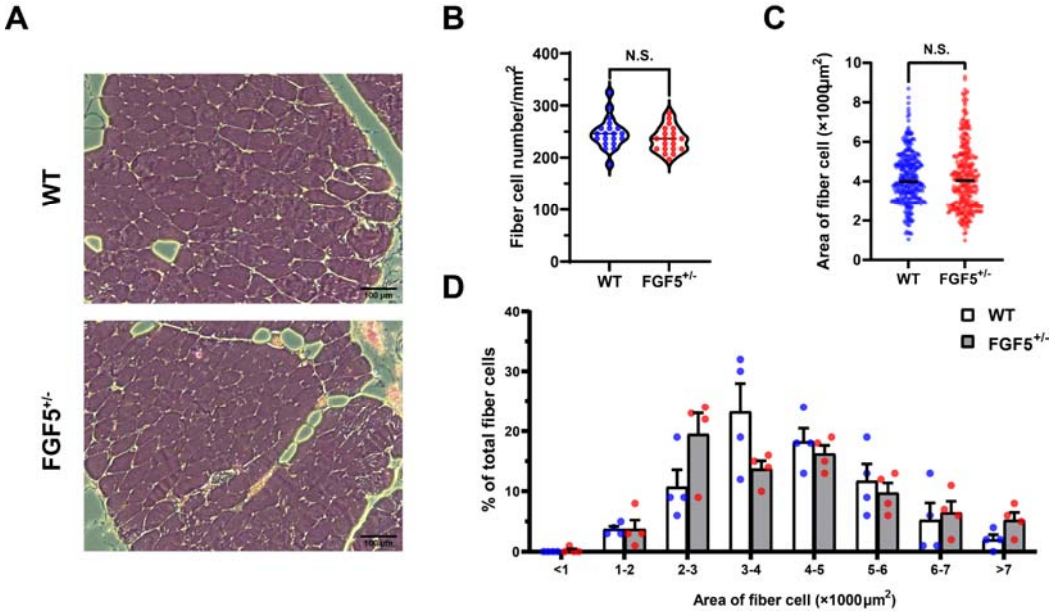

820
821 (A) HE sections of gluteus medius in WT and *FGF5*$^{+/-}$ sheep. Scale bar 100 μm. (B)
822 Quantification of muscle fibre cell area of gluteus medius in WT and *FGF5*$^{+/-}$ sheep.
823 (C) Quantification of muscle fibre cell number of per unit area in WT and *FGF5*$^{+/-}$
824 sheep. (D) The percentage of cross-sectional area of different size muscle fibers
825
826

827 **Figure S2 Genotype identification of F1 generation MF$^{+/-}$ sheep**

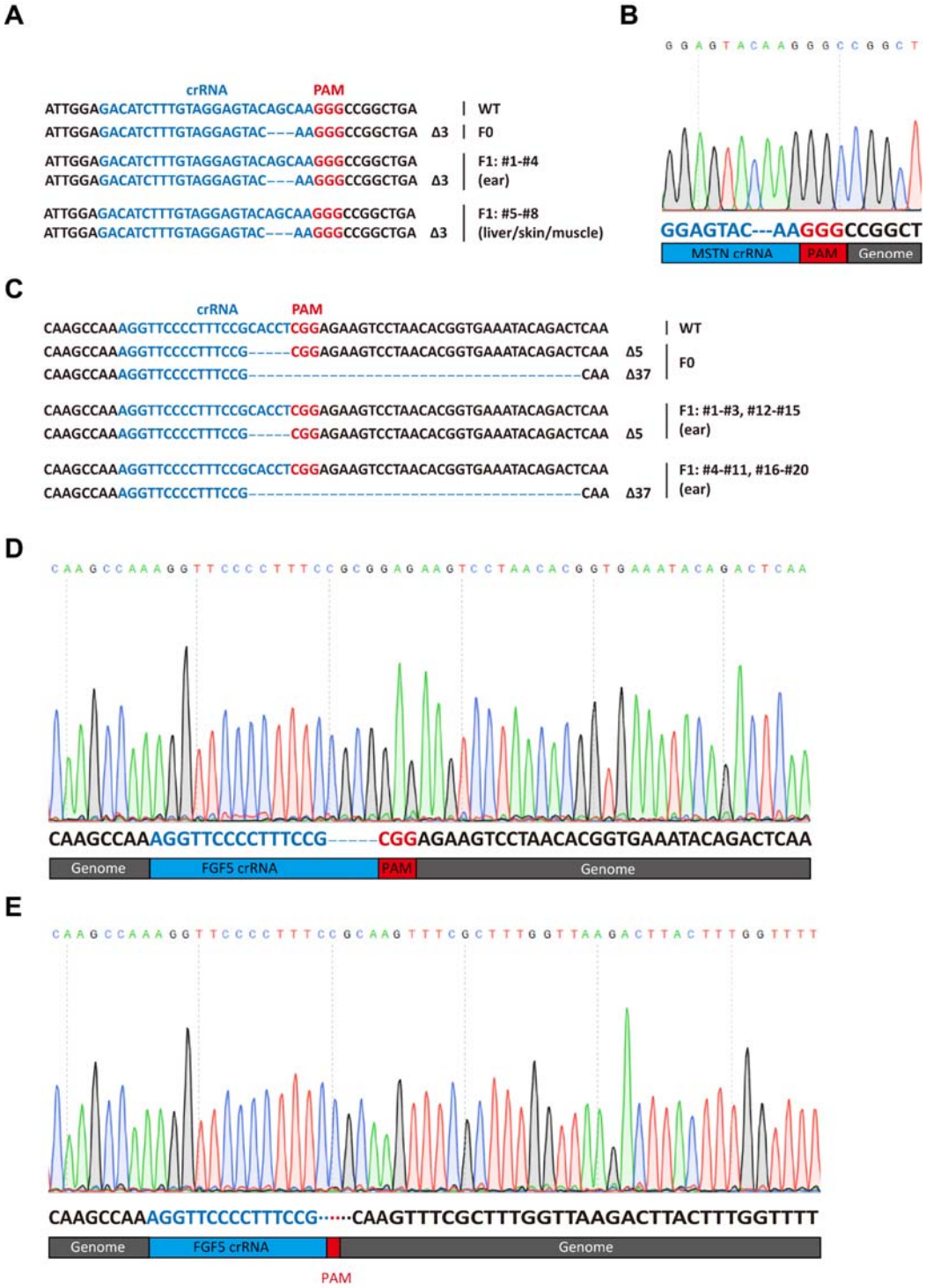

828

829 (A) Identification of *MSTN* mutation type. The ear, liver, skin and muscle tissues of
830 F1 generation MF$^{+/-}$ sheep were selected to identify the genotype of MSTN. (B)
831 *MSTN* mutation sequencing peak. (C) Identification of *FGF5* mutation type. The ear

832 tissue of F1 generation $MF^{+/-}$ sheep was selected to identify the genotype of *FGF5*.
833 (D-E) *FGF5* mutation sequencing peak.
834
835 **Figure S3 The *MSTN*^{Del273C} mutation with *FGF5* knockout has no potential effect**
836 **on MSTN expression**

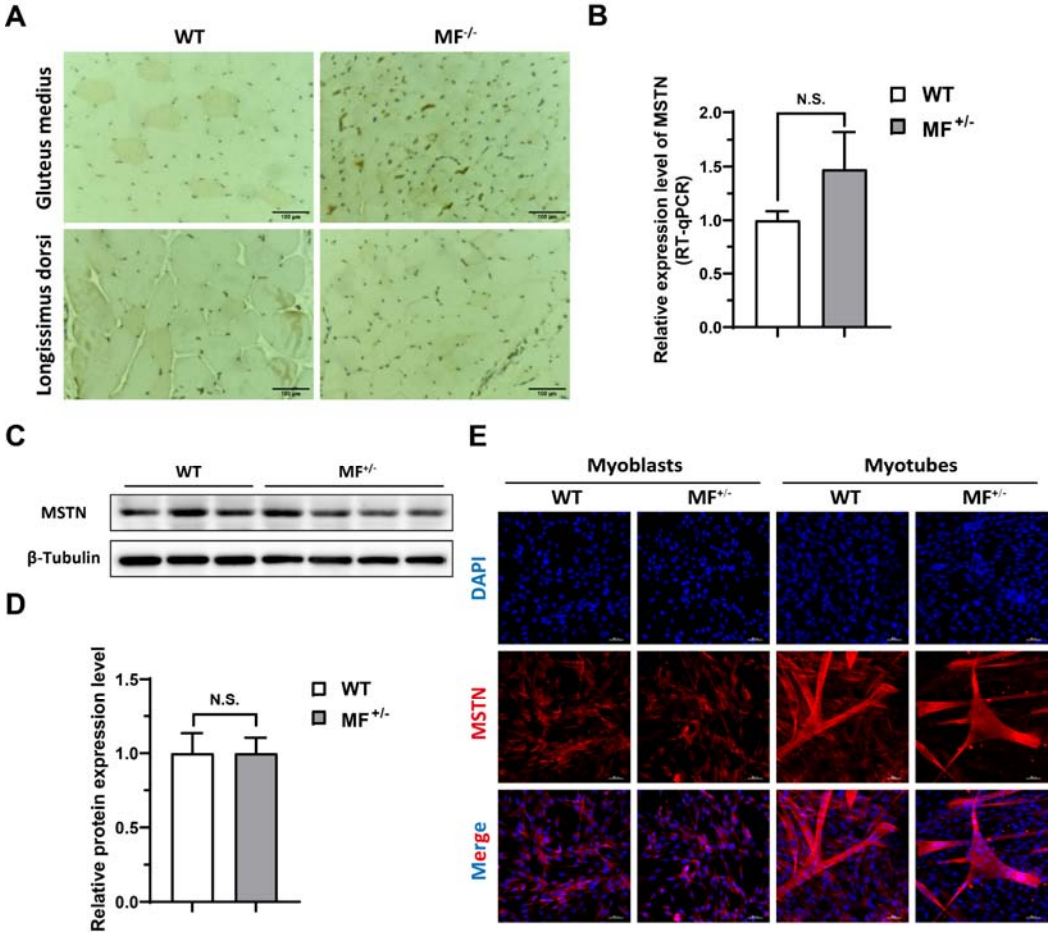

837
838 (A) MSTN immunohistochemistry of gluteus medius and longissimus dorsi in WT
839 and $MF^{-/-}$ sheep. (B) MSTN mRNA expression level of gluteus medius in WT and
840 $MF^{+/-}$ sheep. (C-D) MSTN protein expression level of gluteus medius in WT and
841 $MF^{+/-}$ sheep. (E) MSTN immunofluorescence staining in myoblasts and myotubes of
842 WT and $MF^{+/-}$ sheep.
843
844

845 **Figure S4 The myogenic differentiation ability of MF$^{+/-}$ cells was continuously**
846 **inhibited**

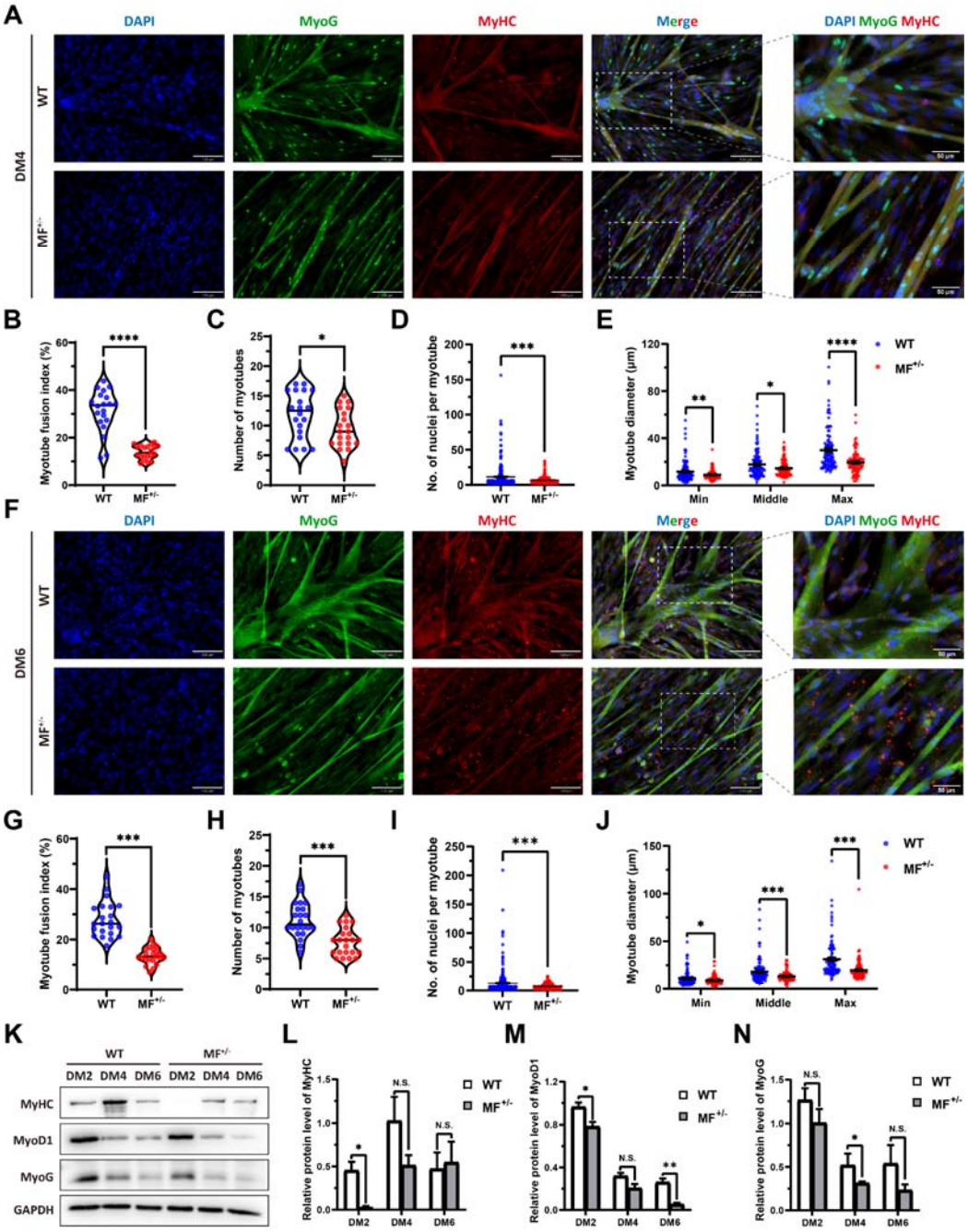

847

848 (A) The MyoG and MyHC immunofluorescence staining of myotubes in DM4. Scale
849 bar 130 μm. (B-E) The myotube fusion index, number of myotubes, number of nuclei
850 per myotube and the myotube diameter in DM4. (F) The MyoG and MyHC
851 immunofluorescence staining of myotubes in DM6. Scale bar 130 μm. (G-J) The
852 myotube fusion index, number of myotubes, number of nuclei per myotube and the

853 myotube diameter in DM6. (K) The protein expression levels of myogenic
854 differentiation marker genes and potential regulator FOSL1 and its family member
855 c-Fos during myogenic differentiation. (L-N) Quantification of protein levels of
856 myogenic differentiation marker genes.
857
858 **Figure S5 The expression of DEGs at different levels**

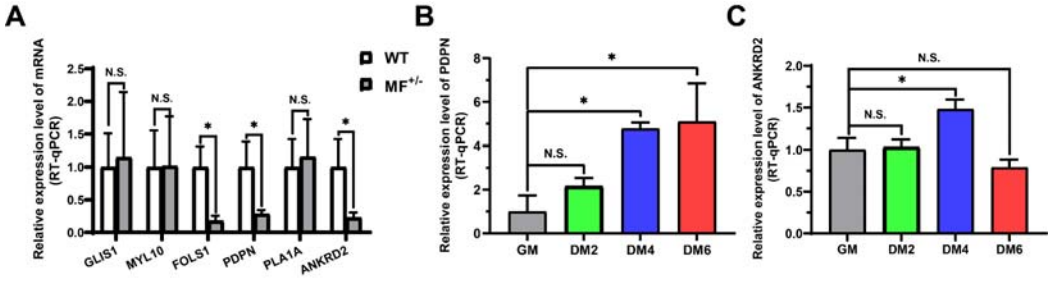

859
860 (A) The expression level of DEGs in the longissimus dorsi. (B) The expression level
861 of PDPN mRNA during myogenic differentiation. (C) The expression level of
862 ANKRD2 mRNA during myogenic differentiation.
863

References

Alli, N. S., Yang, E. C., Miyake, T., Aziz, A., Collins-Hooper, H., Patel, K. & McDermott, J. C. (2013). Signal-dependent fra-2 regulation in skeletal muscle reserve and satellite cells. *Cell Death Dis* 4: e692.

Baig, M. H., Ahmad, K., Moon, J. S., Park, S. Y., Ho Lim, J., Chun, H. J., Qadri, A. F., Hwang, Y. C., Jan, A. T., Ahmad, S. S., Ali, S., Shaikh, S., Lee, E. J. & Choi, I. (2022). Myostatin and its Regulation: A Comprehensive Review of Myostatin Inhibiting Strategies. *Front Physiol* 13: 876078.

Bao, D., Ma, Y., Zhang, X., Guan, F., Chen, W., Gao, K., Qin, C. & Zhang, L. (2015). Preliminary Characterization of a Leptin Receptor Knockout Rat Created by CRISPR/Cas9 System. *Sci Rep* 5: 15942.

Bengal, E., Ransone, L., Scharfmann, R., Dwarki, V. J., Tapscott, S. J., Weintraub, H. & Verma, I. M. (1992). Functional antagonism between c-Jun and MyoD proteins: a direct physical association. *Cell* 68(3): 507-519.

Boman, I. A., Klemetsdal, G., Blichfeldt, T., Nafstad, O. & Vage, D. I. (2009). A frameshift mutation in the coding region of the myostatin gene (MSTN) affects carcass conformation and fatness in Norwegian White Sheep (Ovis aries). *Anim Genet* 40(4): 418-422.

Boman, I. A. & Vage, D. I. (2009). An insertion in the coding region of the myostatin (MSTN) gene affects carcass conformation and fatness in the Norwegian Spaelsau (Ovis aries). *BMC Res Notes* 2: 98.

Braun, T. & Gautel, M. (2011). Transcriptional mechanisms regulating skeletal muscle differentiation, growth and homeostasis. *Nat Rev Mol Cell Biol* 12(6): 349-361.

Chen, M., Zhang, L., Guo, Y., Liu, X., Song, Y., Li, X., Ding, X. & Guo, H. (2021a). A novel lncRNA promotes myogenesis of bovine skeletal muscle satellite cells via PFN1-RhoA/Rac1. *J Cell Mol Med*.

Chen, M. M., Zhao, Y. P., Zhao, Y., Deng, S. L. & Yu, K. (2021b). Regulation of Myostatin on the Growth and Development of Skeletal Muscle. *Front Cell Dev Biol* 9: 785712.

Chen, Y., Zheng, Y., Kang, Y., Yang, W., Niu, Y., Guo, X., Tu, Z., Si, C., Wang, H., Xing, R., Pu, X., Yang, S. H., Li, S., Ji, W. & Li, X. J. (2015). Functional disruption of the dystrophin gene in rhesus monkey using CRISPR/Cas9. *Hum Mol Genet* 24(13): 3764-3774.

Dehnavi, E., Ahani Azari, M., Hasani, S., Nassiry, M. R., Mohajer, M., Khan Ahmadi, A., Shahmohamadi, L. & Yousefi, S. (2012). Polymorphism of Myostatin Gene in Intron 1 and 2 and Exon 3, and Their Associations with Yearling Weight, Using PCR-RFLP and PCR-SSCP Techniques in Zel Sheep. *Biotechnol Res Int* 2012: 472307.

Dierks, C., Momke, S., Philipp, U. & Distl, O. (2013). Allelic heterogeneity of FGF5 mutations causes the long-hair phenotype in dogs. *Anim Genet* 44(4): 425-431.

Dilger, A. C., Gabriel, S. R., Kutzler, L. W., McKeith, F. K. & Killefer, J. (2010). The myostatin null mutation and clenbuterol administration elicit additive effects in mice. *Animal* 4(3): 466-471.

Fan, Z., Liu, Z., Xu, K., Wu, T., Ruan, J., Zheng, X., Bao, S., Mu, Y., Sonstegard, T. & Li, K. (2022). Long-term, multidomain analyses to identify the breed and allelic effects in MSTN-edited pigs to overcome lameness and sustainably improve nutritional meat production. *Sci China Life Sci* 65(2): 362-375.

Gao, L., Yang, M., Wei, Z., Gu, M., Yang, L., Bai, C., Wu, Y. & Li, G. (2020). MSTN Mutant Promotes Myogenic Differentiation by Increasing Demethylase TET1 Expression via the SMAD2/SMAD3 Pathway. *Int J Biol Sci* 16(8): 1324-1334.

Ge, L., Dong, X., Gong, X., Kang, J., Zhang, Y. & Quan, F. (2020). Mutation in myostatin 3'UTR promotes C2C12 myoblast proliferation and differentiation by blocking the translation of MSTN. *Int J Biol Macromol* 154: 634-643.

Grisolia, A. B., D'Angelo, G. T., Porto Neto, L. R., Siqueira, F. & Garcia, J. F. (2009). Myostatin (GDF8) single nucleotide polymorphisms in Nellore cattle. *Genet Mol Res* 8(3): 822-830.

Grobet, L., Martin, L. J., Poncelet, D., Pirottin, D., Brouwers, B., Riquet, J., Schoeberlein, A., Dunner, S., Menissier, F., Massabanda, J., Fries, R., Hanset, R. & Georges, M. (1997). A deletion in the bovine myostatin gene causes the double-muscled phenotype in cattle. *Nat Genet* 17(1): 71-74.

Gui, T., Sun, Y., Shimokado, A. & Muragaki, Y. (2012). The Roles of Mitogen-Activated Protein Kinase Pathways in TGF-beta-Induced Epithelial-Mesenchymal Transition. *J Signal Transduct* 2012: 289243.

Hai, T., Teng, F., Guo, R., Li, W. & Zhou, Q. (2014). One-step generation of knockout pigs by zygote injection of CRISPR/Cas system. *Cell Res* 24(3): 372-375.

Haidet, A. M., Rizo, L., Handy, C., Umapathi, P., Eagle, A., Shilling, C., Boue, D., Martin, P. T., Sahenk, Z., Mendell, J. R. & Kaspar, B. K. (2008). Long-term enhancement of skeletal muscle mass and strength by single gene administration of myostatin inhibitors. *Proc Natl Acad Sci U S A* 105(11): 4318-4322.

Han, J., Forrest, R. H. & Hickford, J. G. (2013). Genetic variations in the myostatin gene (MSTN) in New Zealand sheep breeds. *Mol Biol Rep* 40(11): 6379-6384.

Hanset, R. & Michaux, C. (1985). On the genetic determinism of muscular hypertrophy in the Belgian White and Blue cattle breed. I. Experimental data. *Genet Sel Evol (1983)* 17(3): 359-368.

Hebert, J. M., Rosenquist, T., Gotz, J. & Martin, G. R. (1994). FGF5 as a regulator of the hair growth cycle: evidence from targeted and spontaneous mutations. *Cell* 78(6): 1017-1025.

Higgins, C. A., Petukhova, L., Harel, S., Ho, Y. Y., Drill, E., Shapiro, L., Wajid, M. & Christiano, A. M. (2014). FGF5 is a crucial regulator of hair length in humans. *Proc Natl Acad Sci U S A* 111(29): 10648-10653.

Hongbing HAN, Y. M., Tao WANG,Ling LIAN,Xiuzhi TIAN,Rui HU,Shoulong DENG,Kongpan LI,Feng WANG,Ning LI,Guoshi LIU,Yaofeng ZHAO,Zhengxing LIAN (2014). One-step generation of myostatin gene knockout sheep via the CRISPR/Cas9 system. *Front. Agr. Sci. Eng.* 1(1): 2-5.

Huang, Z., Chen, D., Zhang, K., Yu, B., Chen, X. & Meng, J. (2007). Regulation of myostatin signaling by c-Jun N-terminal kinase in C2C12 cells. *Cell Signal* 19(11): 2286-2295.

Joulia, D., Bernardi, H., Garandel, V., Rabenoelina, F., Vernus, B. & Cabello, G. (2003). Mechanisms involved in the inhibition of myoblast proliferation and differentiation by myostatin. *Experimental cell research* 286(2): 263-275.

Kambadur, R., Sharma, M., Smith, T. P. & Bass, J. J. (1997). Mutations in myostatin (GDF8) in double-muscled Belgian Blue and Piedmontese cattle. *Genome Res* 7(9): 910-916.

Kehler, J. S., David, V. A., Schaffer, A. A., Bajema, K., Eizirik, E., Ryugo, D. K., Hannah, S. S., O'Brien, S. J. & Menotti-Raymond, M. (2007). Four independent mutations in the feline fibroblast growth factor 5 gene determine the long-haired phenotype in domestic cats. *J Hered* 98(6): 555-566.

Kijas, J. W., McCulloch, R., Edwards, J. E., Oddy, V. H., Lee, S. H. & van der Werf, J. (2007). Evidence for multiple alleles effecting muscling and fatness at the ovine GDF8 locus. *BMC Genet* 8: 80.

Kotani, H., Taimatsu, K., Ohga, R., Ota, S. & Kawahara, A. (2015). Efficient Multiple Genome Modifications Induced by the crRNAs, tracrRNA and Cas9 Protein Complex in Zebrafish. *PLoS One* 10(5): e0128319.

Lamarche, E., AlSudais, H., Rajgara, R., Fu, D., Omaiche, S. & Wiper-Bergeron, N. (2021). SMAD2 promotes myogenin expression and terminal myogenic differentiation. *Development* 148(3).

Langley, B., Thomas, M., Bishop, A., Sharma, M., Gilmour, S. & Kambadur, R. (2002). Myostatin inhibits myoblast differentiation by down-regulating MyoD expression. *J Biol Chem* 277(51): 49831-49840.

975 Lee, S. J. (2021). Targeting the myostatin signaling pathway to treat muscle loss and
976 metabolic dysfunction. *J Clin Invest* 131(9).
977 Legrand, R., Tiret, L. & Abitbol, M. (2014). Two recessive mutations in FGF5 are
978 associated with the long-hair phenotype in donkeys. *Genet Sel Evol* 46: 65.
979 Li, L., Chambard, J. C., Karin, M. & Olson, E. N. (1992). Fos and Jun repress
980 transcriptional activation by myogenin and MyoD: the amino terminus of Jun
981 can mediate repression. *Genes Dev* 6(4): 676-689.
982 Liu, X., Manzano, G., Lovett, D. H. & Kim, H. T. (2010). Role of AP-1 and RE-1
983 binding sites in matrix metalloproteinase-2 transcriptional regulation in
984 skeletal muscle atrophy. *Biochem Biophys Res Commun* 396(2): 219-223.
985 Lv, Q., Yuan, L., Deng, J., Chen, M., Wang, Y., Zeng, J., Li, Z. & Lai, L. (2016).
986 Efficient Generation of Myostatin Gene Mutated Rabbit by CRISPR/Cas9. *Sci*
987 *Rep* 6: 25029.
988 Marchitelli, C., Savarese, M. C., Crisa, A., Nardone, A., Marsan, P. A. & Valentini, A.
989 (2003). Double muscling in Marchigiana beef breed is caused by a stop codon
990 in the third exon of myostatin gene. *Mamm Genome* 14(6): 392-395.
991 Marques, C., Unterkircher, T., Kroon, P., Oldrini, B., Izzo, A., Dramaretska, Y.,
992 Ferrarese, R., Kling, E., Schnell, O., Nelander, S., Wagner, E. F., Bakiri, L.,
993 Gargiulo, G., Carro, M. S. & Squatrito, M. (2021). NF1 regulates
994 mesenchymal glioblastoma plasticity and aggressiveness through the AP-1
995 transcription factor FOSL1. *Elife* 10.
996 Mathes, S., Fahrner, A., Ghoshdastider, U., Rudiger, H. A., Leunig, M., Wolfrum, C.
997 & Krutzfeldt, J. (2021). FGF-2-dependent signaling activated in aged human
998 skeletal muscle promotes intramuscular adipogenesis. *Proc Natl Acad Sci U S*
999 *A* 118(37).
1000 McCroskery, S., Thomas, M., Maxwell, L., Sharma, M. & Kambadur, R. (2003).
1001 Myostatin negatively regulates satellite cell activation and self-renewal.
1002 *Journal of Cell Biology* 162(6): 1135-1147.
1003 McPherron, A. C., Lawler, A. M. & Lee, S. J. (1997). Regulation of skeletal muscle
1004 mass in mice by a new TGF-beta superfamily member. *Nature* 387(6628):
1005 83-90.
1006 Morissette, M. R., Cook, S. A., Buranasombati, C., Rosenberg, M. A. & Rosenzweig,
1007 A. (2009). Myostatin inhibits IGF-I-induced myotube hypertrophy through
1008 Akt. *Am J Physiol Cell Physiol* 297(5): C1124-1132.
1009 Nishi, M., Yasue, A., Nishimatu, S., Nohno, T., Yamaoka, T., Itakura, M., Moriyama,
1010 K., Ohuchi, H. & Noji, S. (2002). A missense mutant myostatin causes
1011 hyperplasia without hypertrophy in the mouse muscle. *Biochem Biophys Res*
1012 *Commun* 293(1): 247-251.
1013 Niu, Y., Shen, B., Cui, Y., Chen, Y., Wang, J., Wang, L., Kang, Y., Zhao, X., Si, W., Li,
1014 W., Xiang, A. P., Zhou, J., Guo, X., Bi, Y., Si, C., Hu, B., Dong, G., Wang, H.,
1015 Zhou, Z., Li, T., Tan, T., Pu, X., Wang, F., Ji, S., Zhou, Q., Huang, X., Ji, W. &
1016 Sha, J. (2014). Generation of gene-modified cynomolgus monkey via
1017 Cas9/RNA-mediated gene targeting in one-cell embryos. *Cell* 156(4):
1018 836-843.
1019 Pothuraju, M., Mishra, S. K., Kumar, S. N., Mohamed, N. F., Kataria, R. S., Yadav, D.
1020 K. & Arora, R. (2015). Polymorphism in the Coding Region Sequence of Gdf8
1021 Gene in Indian Sheep. *Genetika* 51(11): 1297-1300.
1022 Puntschart, A., Wey, E., Jostarndt, K., Vogt, M., Wittwer, M., Widmer, H. R.,
1023 Hoppeler, H. & Billeter, R. (1998). Expression of fos and jun genes in human
1024 skeletal muscle after exercise. *Am J Physiol* 274(1): C129-137.
1025 Qian, L., Tang, M., Yang, J., Wang, Q., Cai, C., Jiang, S., Li, H., Jiang, K., Gao, P.,
1026 Ma, D., Chen, Y., An, X., Li, K. & Cui, W. (2015). Targeted mutations in
1027 myostatin by zinc-finger nucleases result in double-muscled phenotype in
1028 Meishan pigs. *Sci Rep* 5: 14435.
1029 Sato, M., Koriyama, M., Watanabe, S., Ohtsuka, M., Sakurai, T., Inada, E., Saitoh, I.,
1030 Nakamura, S. & Miyoshi, K. (2015). Direct Injection of
1031 CRISPR/Cas9-Related mRNA into Cytoplasm of Parthenogenetically

Activated Porcine Oocytes Causes Frequent Mosaicism for Indel Mutations. *Int J Mol Sci* 16(8): 17838-17856.

Sjakste, T., Paramonova, N., Grislis, Z., Trapina, I. & Kairisa, D. (2011). Analysis of the single-nucleotide polymorphism in the 5'UTR and part of intron I of the sheep MSTN gene. *DNA Cell Biol* 30(7): 433-444.

Sobolev, V. V., Khashukoeva, A. Z., Evina, O. E., Geppe, N. A., Chebysheva, S. N., Korsunskaya, I. M., Tchepourina, E. & Mezentsev, A. (2022). Role of the Transcription Factor FOSL1 in Organ Development and Tumorigenesis. *Int J Mol Sci* 23(3).

Sundberg, J. P., Rourk, M. H., Boggess, D., Hogan, M. E., Sundberg, B. A. & Bertolino, A. P. (1997). Angora mouse mutation: altered hair cycle, follicular dystrophy, phenotypic maintenance of skin grafts, and changes in keratin expression. *Vet Pathol* 34(3): 171-179.

Sung, Y. H., Kim, J. M., Kim, H. T., Lee, J., Jeon, J., Jin, Y., Choi, J. H., Ban, Y. H., Ha, S. J., Kim, C. H., Lee, H. W. & Kim, J. S. (2014). Highly efficient gene knockout in mice and zebrafish with RNA-guided endonucleases. *Genome Res* 24(1): 125-131.

Talotta, F., Casalino, L. & Verde, P. (2020). The nuclear oncoprotein Fra-1: a transcription factor knocking on therapeutic applications' door. *Oncogene* 39(23): 4491-4506.

Taylor, W. E., Bhasin, S., Artaza, J., Byhower, F., Azam, M., Willard, D. H., Jr., Kull, F. C., Jr. & Gonzalez-Cadavid, N. (2001). Myostatin inhibits cell proliferation and protein synthesis in C2C12 muscle cells. *Am J Physiol Endocrinol Metab* 280(2): E221-228.

Thomas, M., Langley, B., Berry, C., Sharma, M., Kirk, S., Bass, J. & Kambadur, R. (2000a). Myostatin, a negative regulator of muscle growth, functions by inhibiting myoblast proliferation. *Journal of Biological Chemistry* 275(51): 40235-40243.

Thomas, M., Langley, B., Berry, C., Sharma, M., Kirk, S., Bass, J. & Kambadur, R. (2000b). Myostatin, a negative regulator of muscle growth, functions by inhibiting myoblast proliferation. *J Biol Chem* 275(51): 40235-40243.

Tobin, S. W., Yang, D., Girgis, J., Farahzad, A., Blais, A. & McDermott, J. C. (2016). Regulation of Hspb7 by MEF2 and AP-1: implications for Hspb7 in muscle atrophy. *J Cell Sci* 129(21): 4076-4090.

Tu, Z., Yang, W., Yan, S., Yin, A., Gao, J., Liu, X., Zheng, Y., Zheng, J., Li, Z., Yang, S., Li, S., Guo, X. & Li, X. J. (2017). Promoting Cas9 degradation reduces mosaic mutations in non-human primate embryos. *Sci Rep* 7: 42081.

Wan, H., Feng, C., Teng, F., Yang, S., Hu, B., Niu, Y., Xiang, A. P., Fang, W., Ji, W., Li, W., Zhao, X. & Zhou, Q. (2015). One-step generation of p53 gene biallelic mutant Cynomolgus monkey via the CRISPR/Cas system. *Cell Res* 25(2): 258-261.

Wang, H. & Yang, H. (2019). Gene-edited babies: What went wrong and what could go wrong. *PLoS Biol* 17(4): e3000224.

Wang, H., Yang, H., Shivalila, C. S., Dawlaty, M. M., Cheng, A. W., Zhang, F. & Jaenisch, R. (2013). One-step generation of mice carrying mutations in multiple genes by CRISPR/Cas-mediated genome engineering. *Cell* 153(4): 910-918.

Wang, Q. & McPherron, A. C. (2012). Myostatin inhibition induces muscle fibre hypertrophy prior to satellite cell activation. *J Physiol* 590(9): 2151-2165.

Wang, X., Yu, H., Lei, A., Zhou, J., Zeng, W., Zhu, H., Dong, Z., Niu, Y., Shi, B., Cai, B., Liu, J., Huang, S., Yan, H., Zhao, X., Zhou, G., He, X., Chen, X., Yang, Y., Jiang, Y., Shi, L., Tian, X., Wang, Y., Ma, B., Huang, X., Qu, L. & Chen, Y. (2015). Generation of gene-modified goats targeting MSTN and FGF5 via zygote injection of CRISPR/Cas9 system. *Sci Rep* 5: 13878.

Wang, Y., Ma, C., Sun, Y., Li, Y., Kang, L. & Jiang, Y. (2017). Dynamic transcriptome and DNA methylome analyses on longissimus dorsi to identify genes underlying intramuscular fat content in pigs. *BMC Genomics* 18(1): 780.

Wegner, J., Albrecht, E., Fiedler, I., Teuscher, F., Papstein, H. J. & Ender, K. (2000). Growth- and breed-related changes of muscle fiber characteristics in cattle. *J Anim Sci* 78(6): 1485-1496.

Wijaya, Y. T., Setiawan, T., Sari, I. N., Park, K., Lee, C. H., Cho, K. W., Lee, Y. K., Lim, J. Y., Yoon, J. K., Lee, S. H. & Kwon, H. Y. (2022). Ginsenoside Rd ameliorates muscle wasting by suppressing the signal transducer and activator of transcription 3 pathway. *J Cachexia Sarcopenia Muscle*.

Xu, T. S., Gu, L. H., Zhang, X. H., Ye, B. G., Liu, X. L. & Hou, S. S. (2013). Characterization of myostatin gene (MSTN) of Pekin duck and the association of its polymorphism with breast muscle traits. *Genet Mol Res* 12(3): 3166-3177.

Xu, Y., Liu, H., Pan, H., Wang, X., Zhang, Y., Yao, B., Li, N., Lai, L. & Li, Z. (2020). CRISPR/Cas9-mediated Disruption of Fibroblast Growth Factor 5 in Rabbits Results in a Systemic Long Hair Phenotype by Prolonging Anagen. *Genes (Basel)* 11(3).

Yoshizawa, Y., Wada, K., Shimoi, G., Kameyama, Y., Wakabayashi, Y., Fukuta, K. & Hashizume, R. (2015). A 1-bp deletion in Fgf5 causes male-dominant long hair in the Syrian hamster. *Mamm Genome* 26(11-12): 630-637.

Zhang, R., Li, Y., Jia, K., Xu, X., Li, Y., Zhao, Y., Zhang, X., Zhang, J., Liu, G., Deng, S. & Lian, Z. (2020). Crosstalk between androgen and Wnt/beta-catenin leads to changes of wool density in FGF5-knockout sheep. *Cell Death Dis* 11(5): 407.

Zhiliang, G., Dahai, Z., Ning, L., Hui, L., Xuemei, D. & Changxin, W. (2004). The single nucleotide polymorphisms of the chicken myostatin gene are associated with skeletal muscle and adipose growth. *Sci China C Life Sci* 47(1): 25-30.

Zhou, J., Wang, J., Shen, B., Chen, L., Su, Y., Yang, J., Zhang, W., Tian, X. & Huang, X. (2014). Dual sgRNAs facilitate CRISPR/Cas9-mediated mouse genome targeting. *FEBS J* 281(7): 1717-1725.

Zhu, X., Hadhazy, M., Wehling, M., Tidball, J. G. & McNally, E. M. (2000). Dominant negative myostatin produces hypertrophy without hyperplasia in muscle. *FEBS Lett* 474(1): 71-75.